Electronic Supplementary Material (ESI) for Chemical Communications

Supplementary Material

Synthesis of Heteroatomic Zintl Anions in Liquid Ammonia – the New Highly Charged $[Sn_4Bi_4]^{4-}$ and Fully Ordered $[Sn_2Bi_2]^{2-}$

Ute Friedrich[a], Maria Neumeier[b], Carina Koch[b] and Nikolaus Korber*[a]

[a] Institute for Inorganic Chemistry, Universitätsstraße 31, 93051 Regensburg
[b] Institute for Organic Chemistry, Universitätsstraße 31, 93051 Regensburg
* E-mail: nikolaus.korber@chemie.uni-regensburg.de

Contents

1 Experimental details

All manipulations were performed under argon atmosphere using standard Schlenk or glovebox techniques. Liquid ammonia was dried over elemental potassium for at least 24 h. [18]crown-6 was dried in vacuum and sublimated prior to use.

For the starting materials KSnBi and CsSnBi equimolar amounts of the corresponding elements were weighed into glass ampoules, which were evacuated and sealed. The ampoules were heated to 723 K and kept at this temperature for 24 h. The cooling process was performed with a rate of 150 K/h to room temperature.

367 mg KSnBi or 461 mg CsSnBi, respectively, were dissolved in approximately 15 ml of liquid ammonia together with 132 mg (0.5 mmol) [18]crown-6. Both solutions showed a reddish-brown colour immediately after the addition of liquid ammonia and were stored at 237 K until crystallisation. $[K([18]crown\text{-}6)]_2[Sn_2Bi_2]\cdot 2NH_3$ (**1**) forms in about 20 % and $[Cs([18]crown\text{-}6)]_4[Sn_4Bi_4]\cdot 12NH_3$ (**2**) in about 10 % crystalline yield.

2 Powder diffraction of solid state phases

Powder diffraction data of the solid state phases KSnBi and CsSnBi were collected with a STADI P (Stoe & Cie GmbH) using Cu-$K_{\alpha 1}$-radiation (λ = 1.540598 Å). All samples were filled in glass capillaries (0.3 mm in diameter).

For KSnBi the only crystalline phase identified is KBi_2 (Figure 1). The experimental data were compared to data generated from single crystal data [1].
Due to high absorption and low crystallinity the powder diffraction analysis of CsSnBi failed.

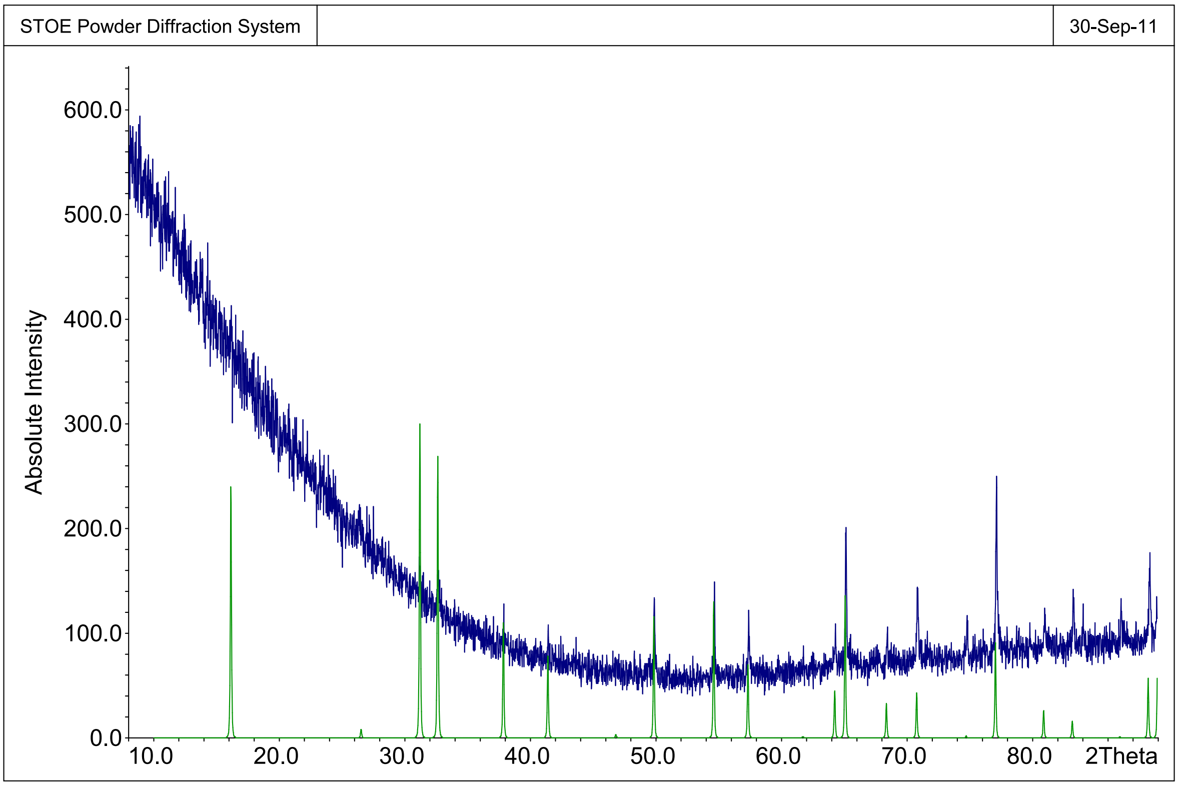

Figure 1 – Experimental diffractogram of KSnBi (blue), showing reflections of KBi_2; generated data green

3 Mass spectrometry analysis

3.1 General

Electrospray Ionization Mass Spectrometry (ESI-MS) was performed on a TSQ 7000 spectrometer by Thermoquest Finnigan in the negative ion mode (Table 1).

The solid state phases were dissolved in less than 1 ml ethylenediamine and diluted with dimethylformamide. An adequate dissolution in pure dimethylformamide could not be observed. The solution of CsSnBi was highly unstable and decayed during the measurement, negatively affecting the profiles of the isotopic pattern. Therefore, additional mass spectrometry investigations were done with [18]crown-6 present in solution. The presence of little amounts of the sequestering agent increased the stability of the solution noticeably, leading to improved mass spectra.

Table 1 – Specific details for ESI-MS

Spray voltage	3 kV	Capillary temperature	200 °C
Capillary voltage	5 V	sheath gas flow rate	80 psi
Tube lens voltage	−95 V		

3.2 ESI mass spectrum of KSnBi in ethylenediamine/dimethylformamide

An overview of the ESI mass spectrum of the solution of KSnBi in ethylenediamine/dimethylformamide is depicted in Figure 2. All fragments observed have been detected as single-charged species. Peaks of identified species (Table 2) are depicted in Figures 3 - 7 together with the simulated isotopic patterns.

Table 2 – Identified fragments in ESI mass spectrum of KSnBi

Species	**m/z**
Sn_9^-	1068.4
Sn_8Bi^-	1158.5
Sn_{10}^-	1187.3
$Sn_7Bi_2^-$	1249.6
$Sn_6Bi_3^-$	1338.7

3 MASS SPECTROMETRY ANALYSIS

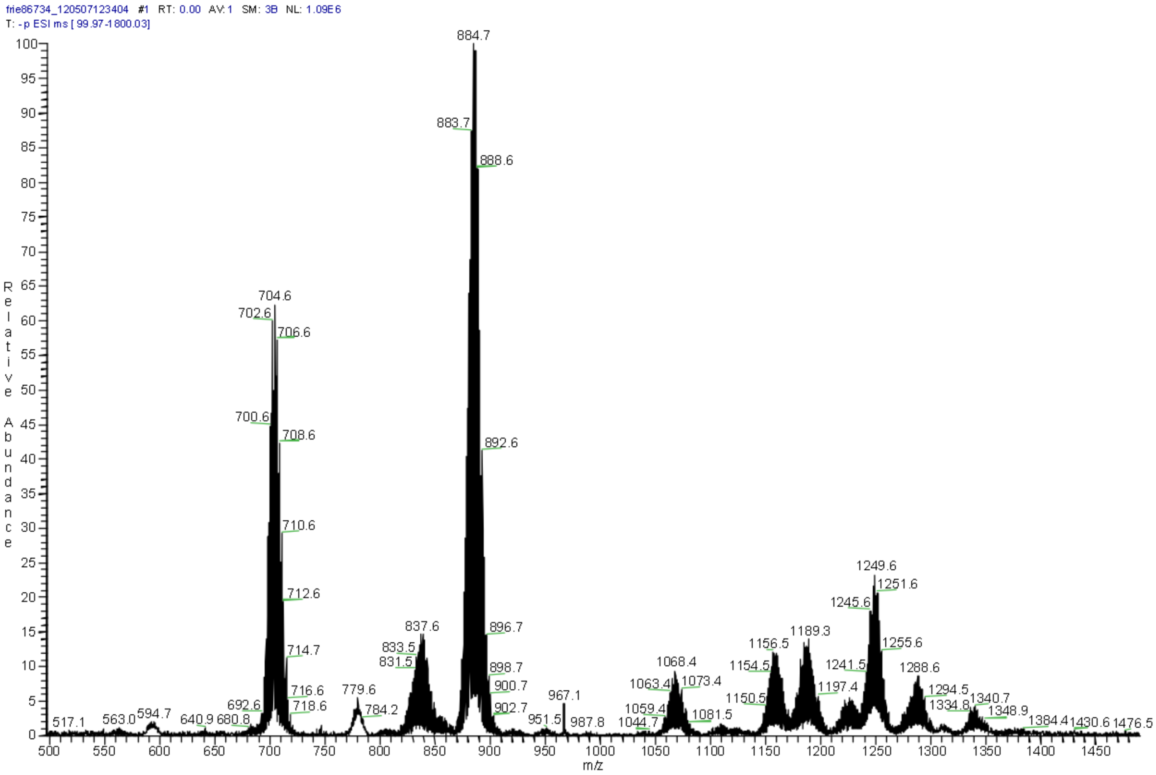

Figure 2 – Overview of the ESI mass spectrum of a solution of KSnBi in a mixture of ethylenediamine/dimethylformamide

3 MASS SPECTROMETRY ANALYSIS

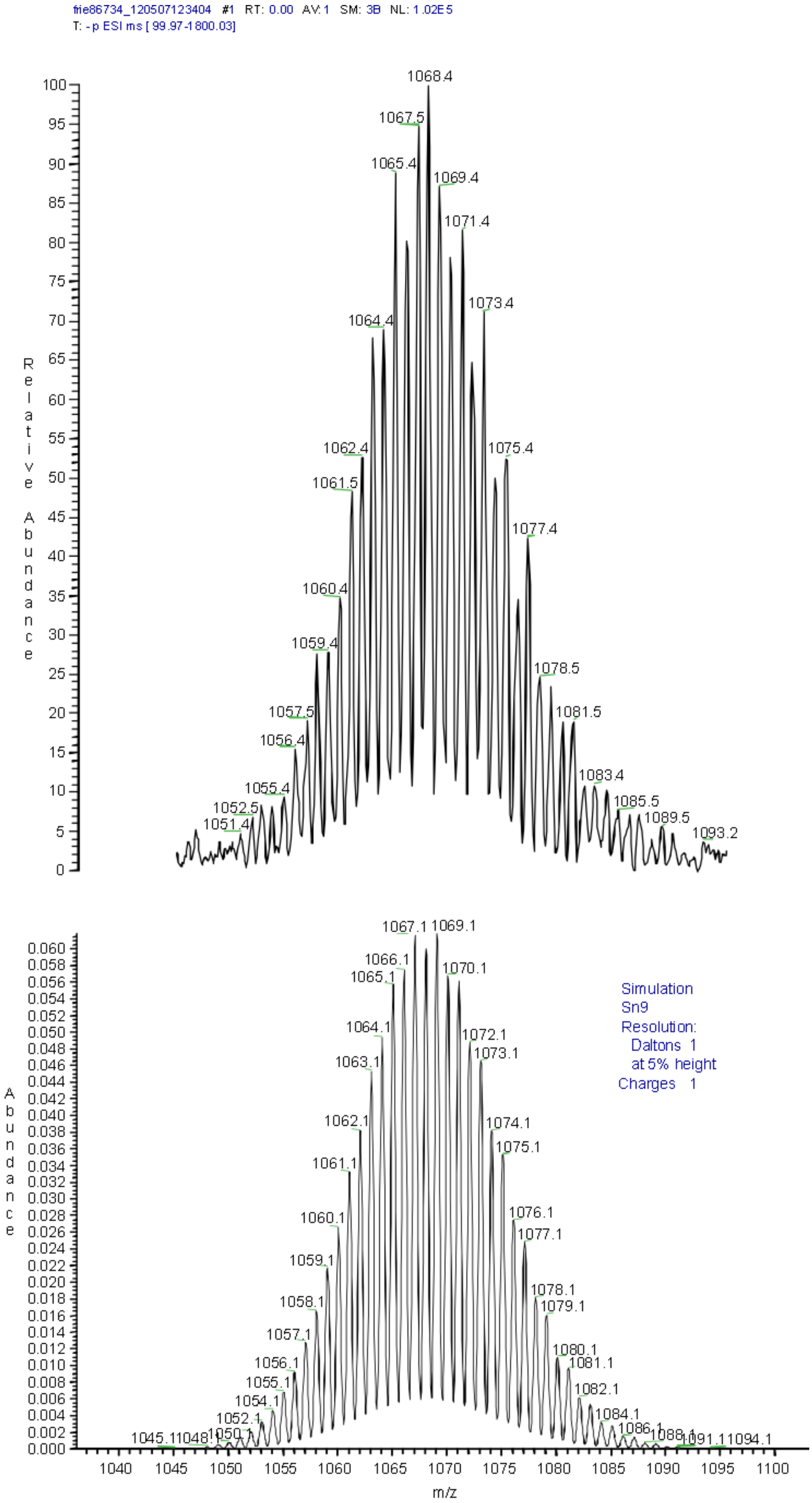

Figure 3 – Measured (top) and simulated (bottom) spectrum of Sn_9^- fragment

3 MASS SPECTROMETRY ANALYSIS

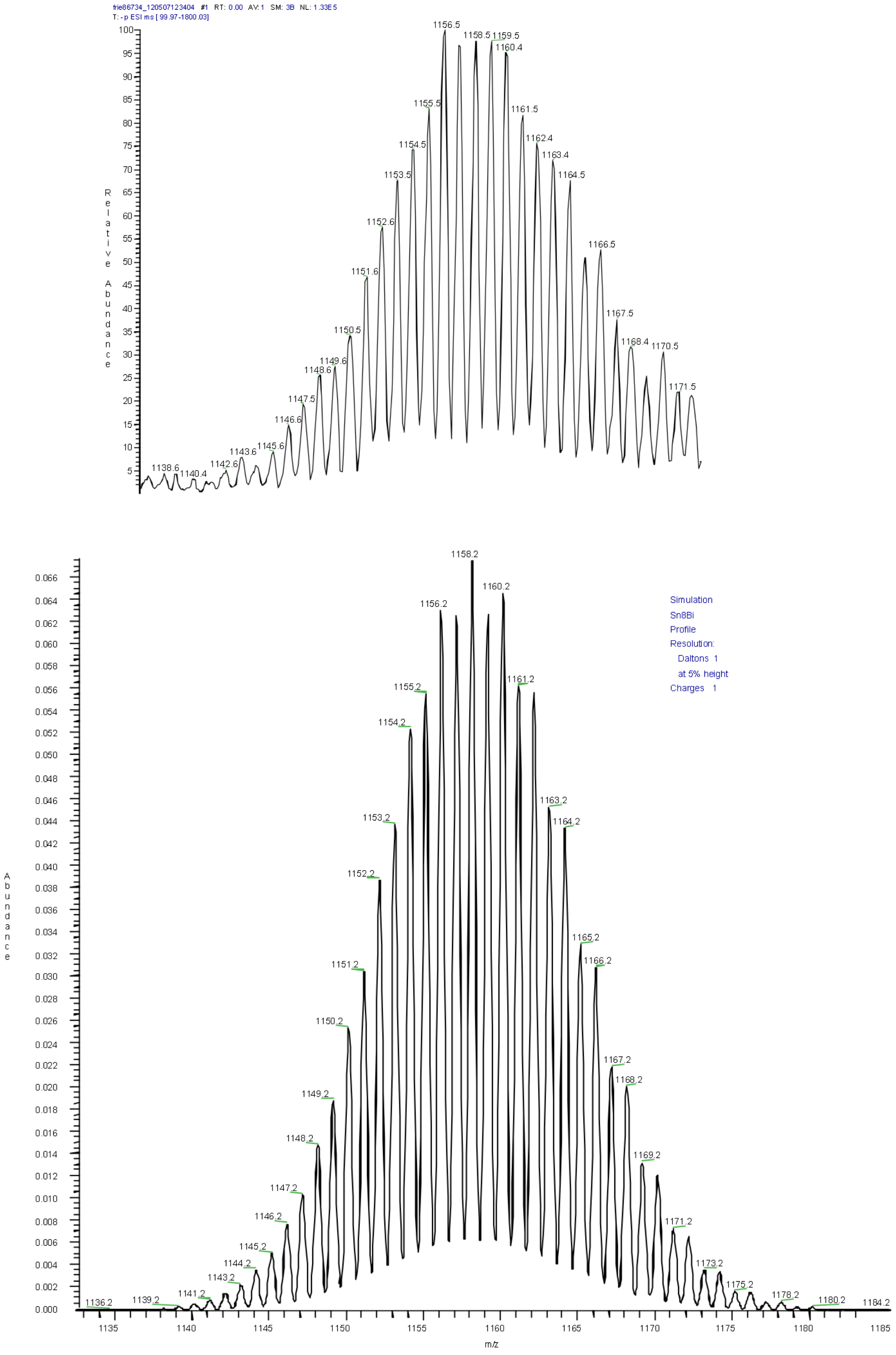

Figure 4 – Measured (top) and simulated (bottom) spectrum of Sn_8Bi^- fragment

3 MASS SPECTROMETRY ANALYSIS

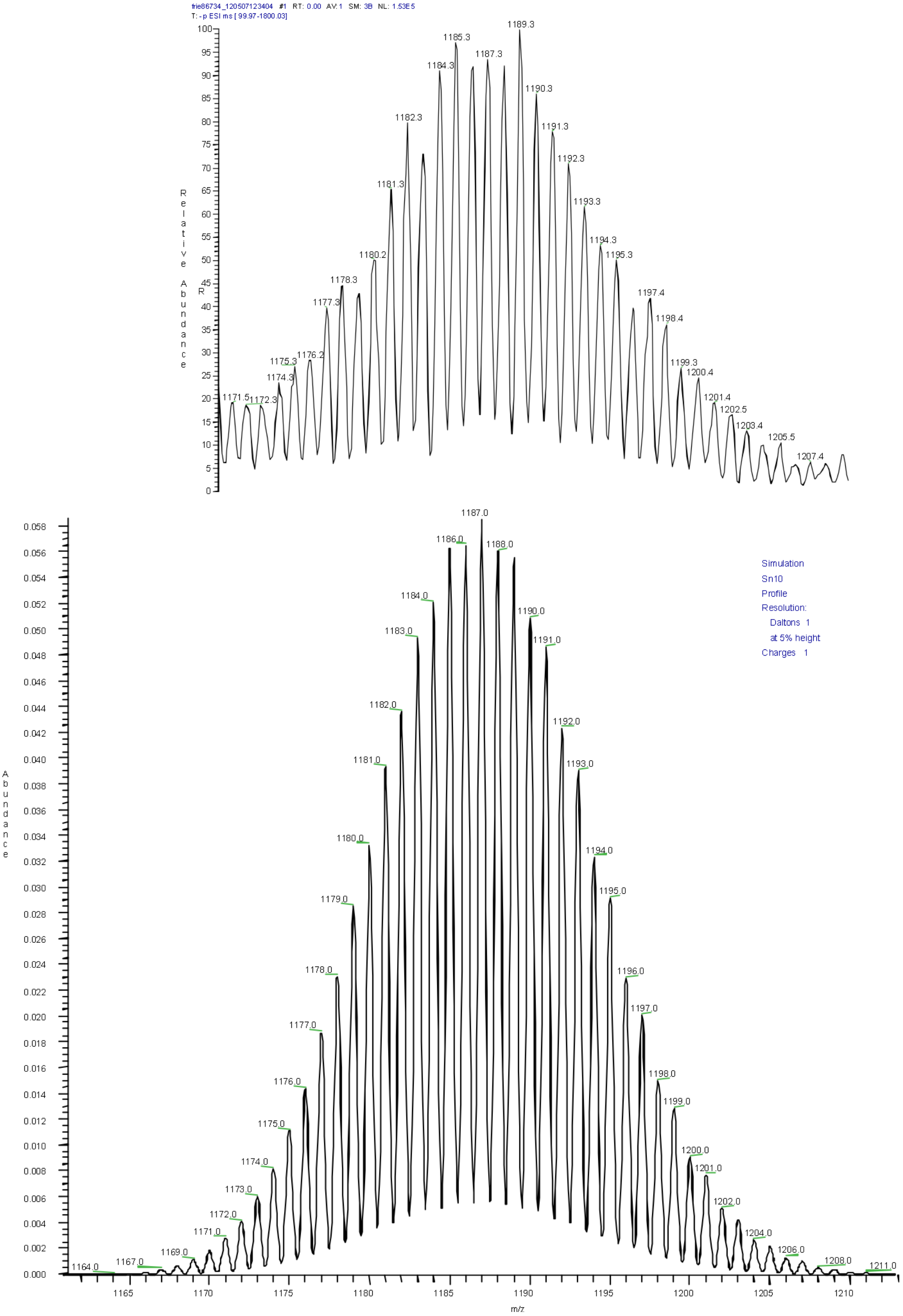

Figure 5 – Measured (top) and simulated (bottom) spectrum of Sn_{10}^{-}-fragment

3 MASS SPECTROMETRY ANALYSIS

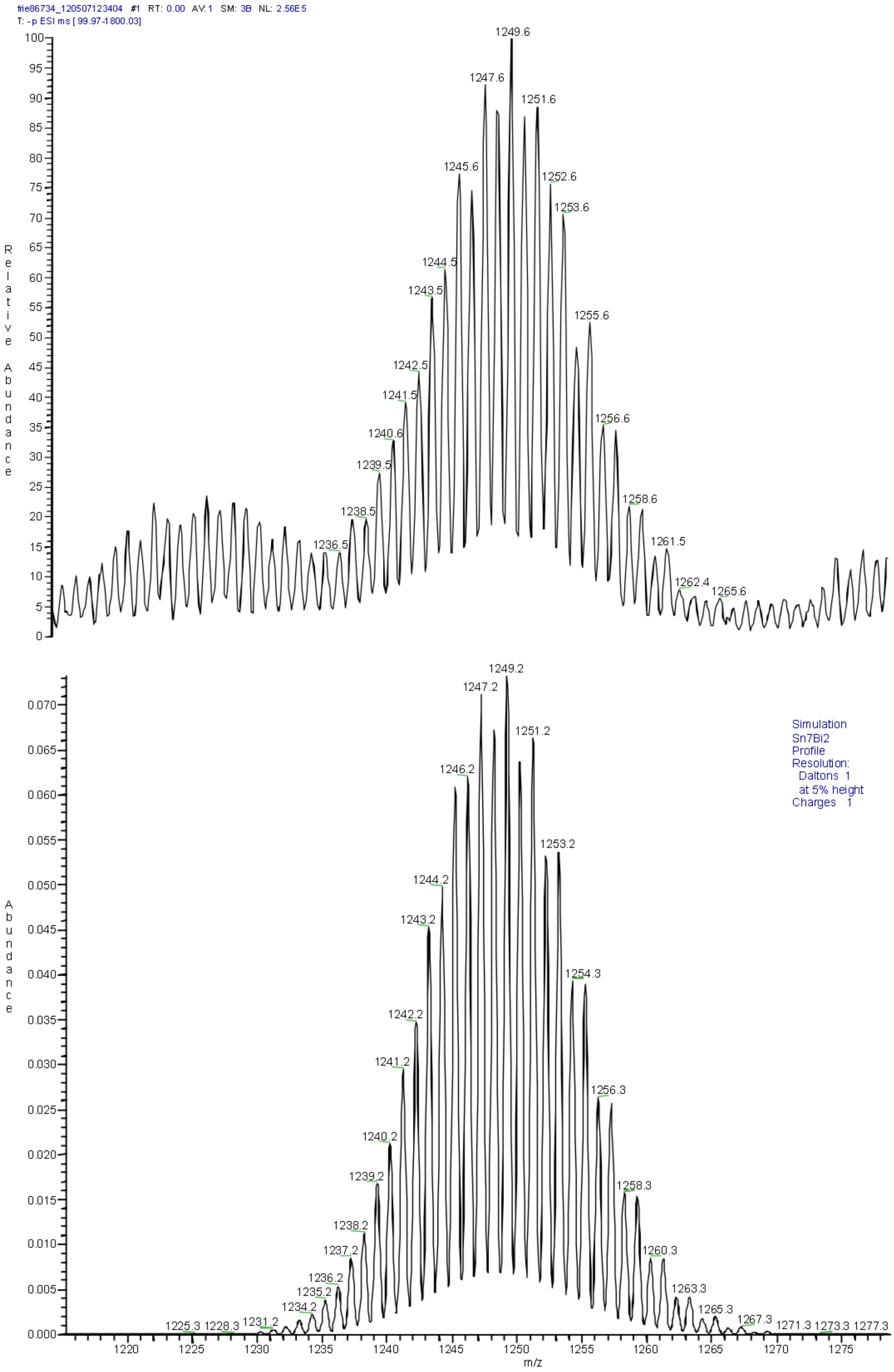

Figure 6 – Measured (top) and simulated (bottom) spectrum of $Sn_7Bi_2^-$ fragment

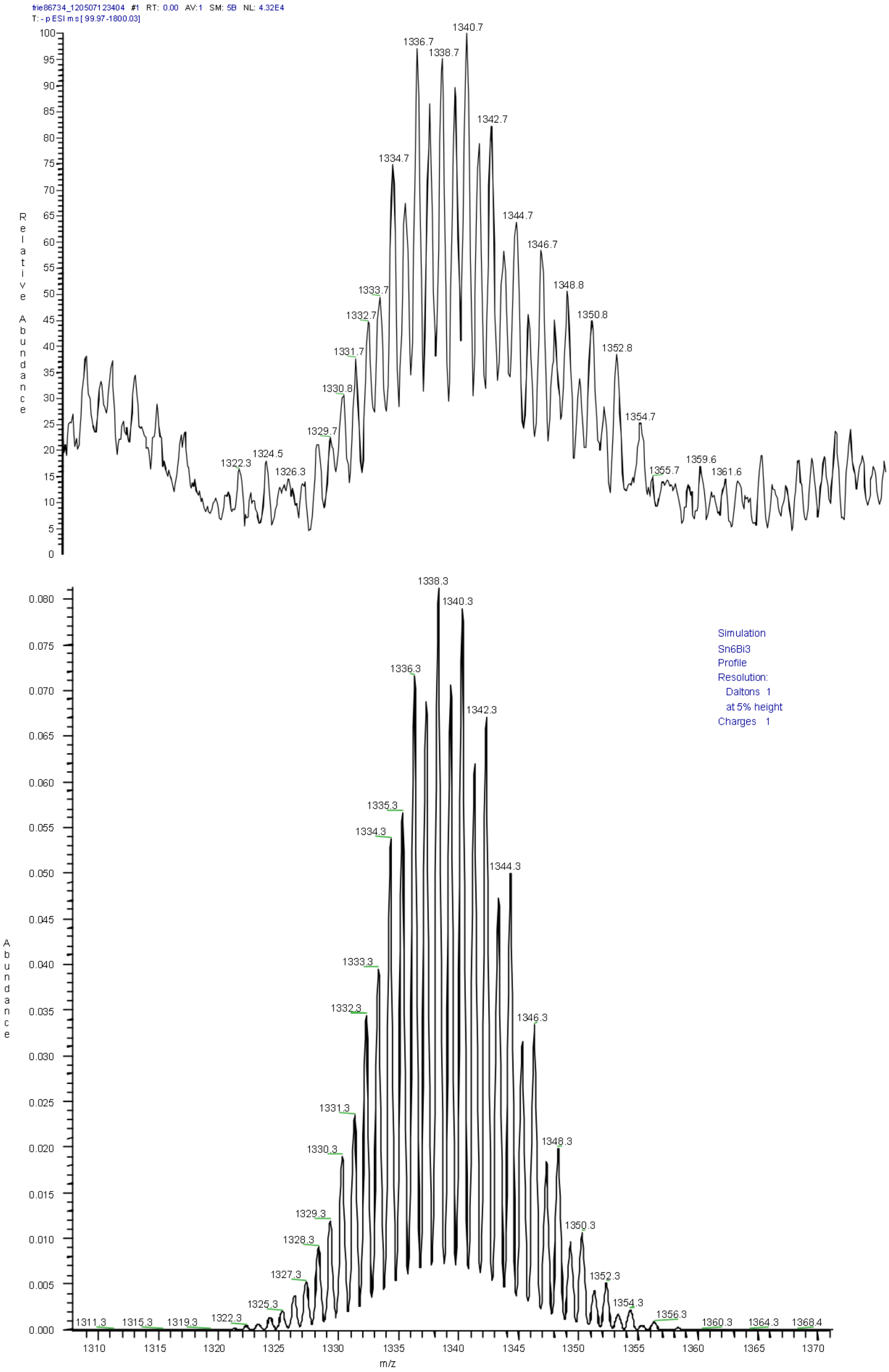

Figure 7 – Measured (top) and simulated (bottom) spectrum of $Sn_6Bi_3^-$ fragment

3.3 ESI mass spectrum of CsSnBi in ethylenediamine/dimethylformamide

An overview of the ESI mass spectrum of the solution of CsSnBi in ethylenediamine/dimethylformamide is depicted in Figure 8. All fragments observed have been detected as single-charged species. Peaks of identified species (Table 3) are shown in Figures 9 - 13 together with the simulated isotopic patterns.

Table 3 – Identified fragments in ESI mass spectrum of CsSnBi

Species	**m/z**
Sn_9^-	1068.5
Sn_8Bi^-	1158.6
Sn_{10}^-	1187.4
$Sn_7Bi_2^-$	1249.6
$Sn_6Bi_3^-$	1338.8

3 MASS SPECTROMETRY ANALYSIS

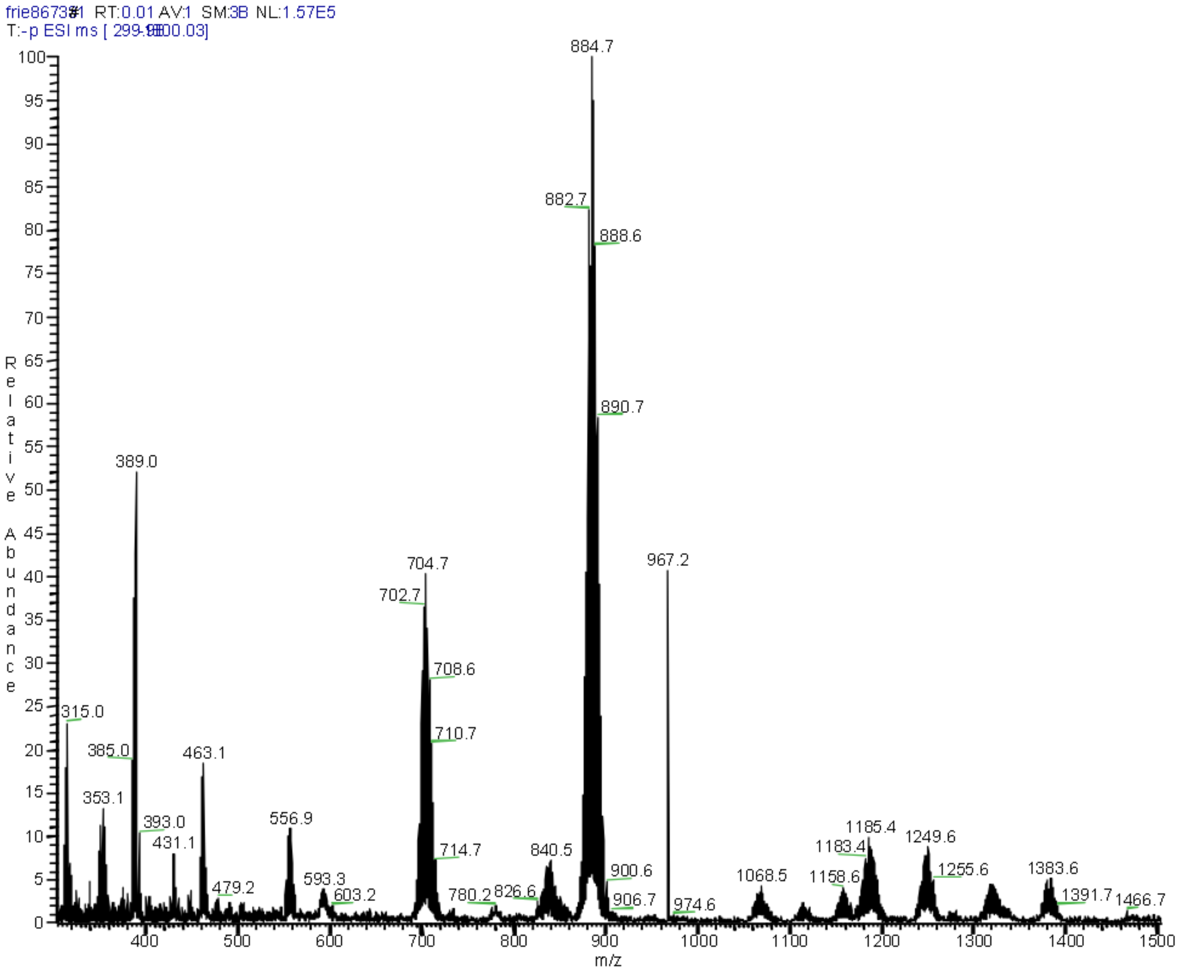

Figure 8 – ESI mass spectrum of a solution of CsSnBi in a mixture of ethylenediamine/dimethylformamide

3 MASS SPECTROMETRY ANALYSIS

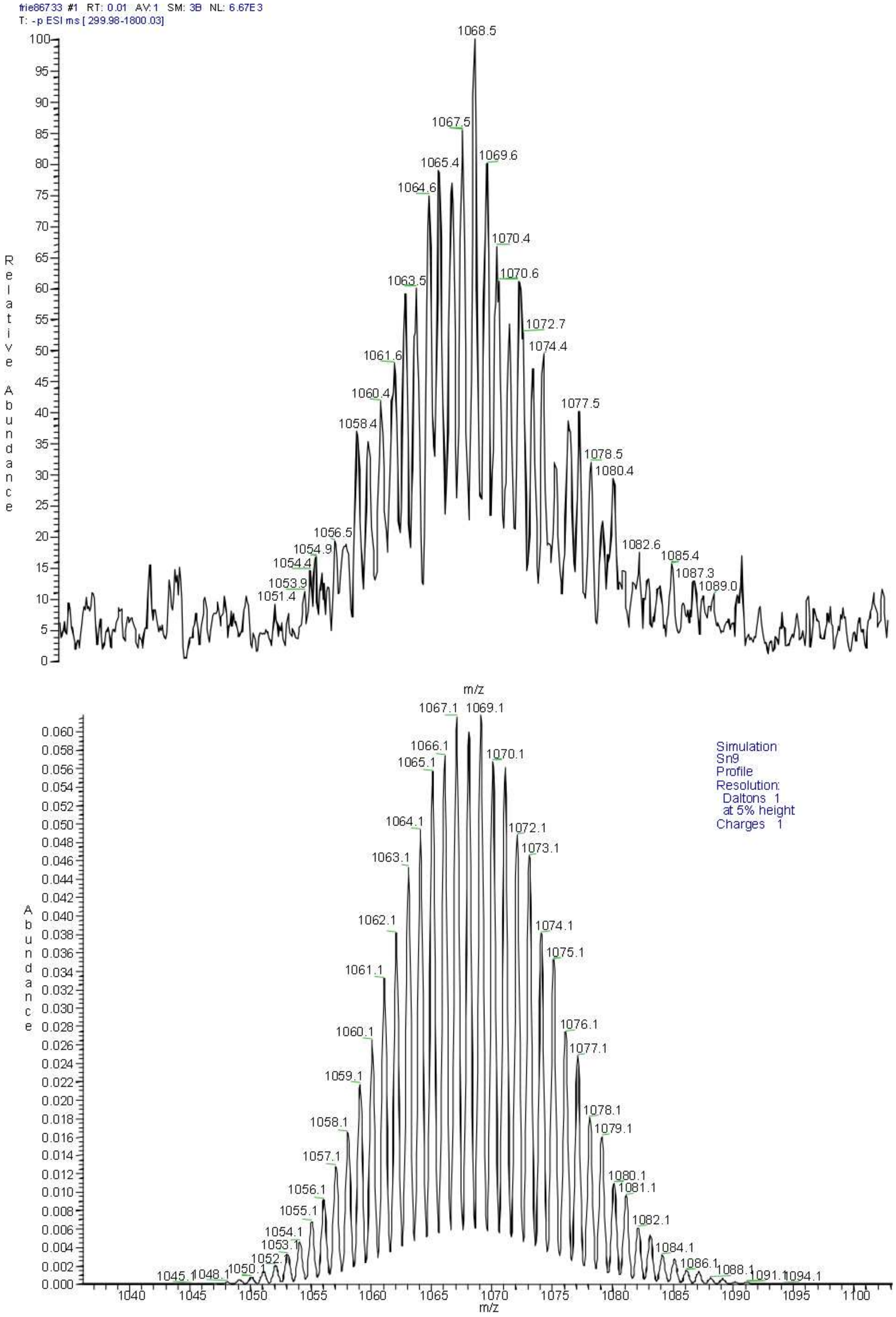

Figure 9 – Measured (top) and simulated (bottom) spectrum of Sn_9^- fragment

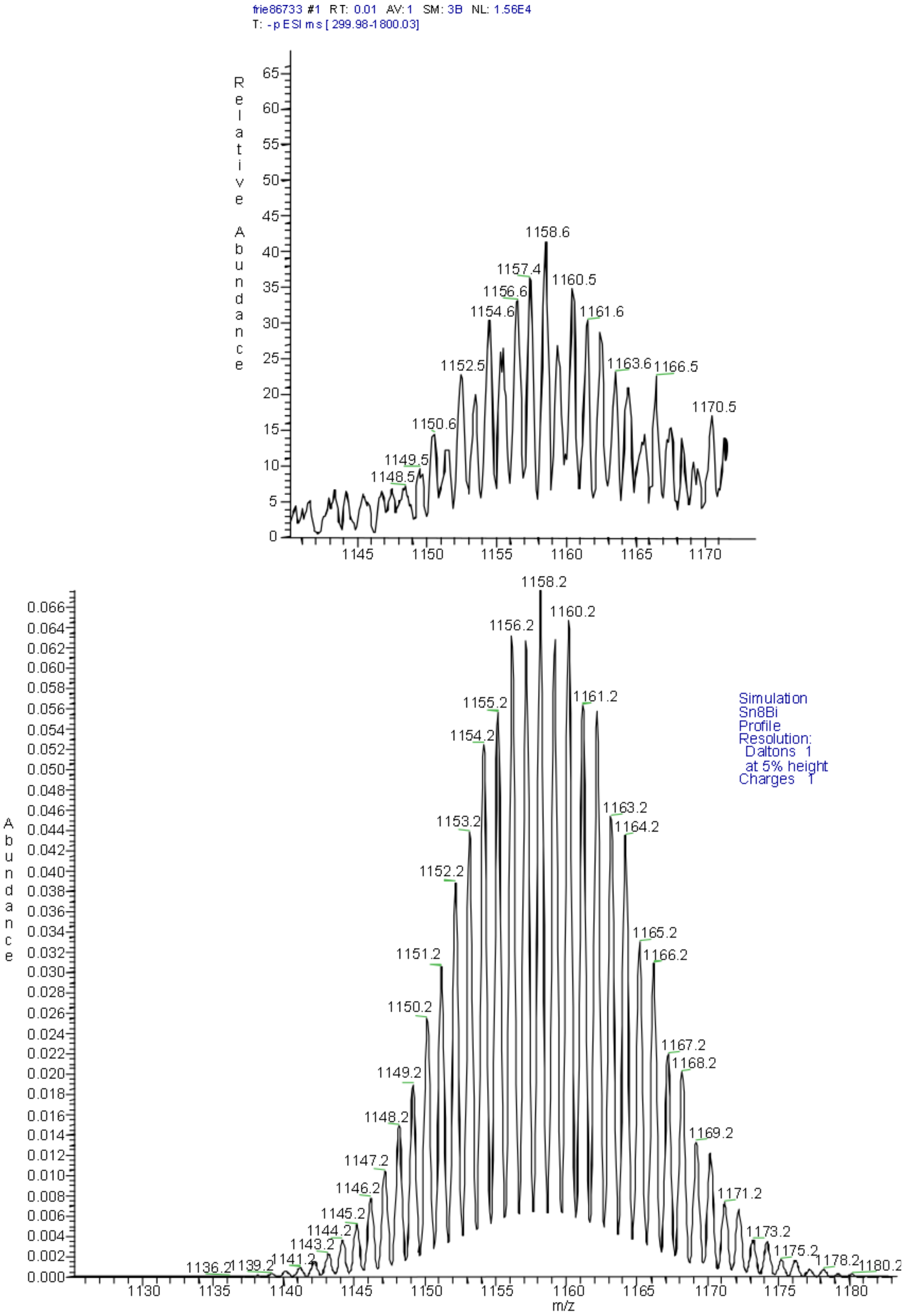

Figure 10 – Measured (top) and simulated (bottom) spectrum of Sn_8Bi^- fragment

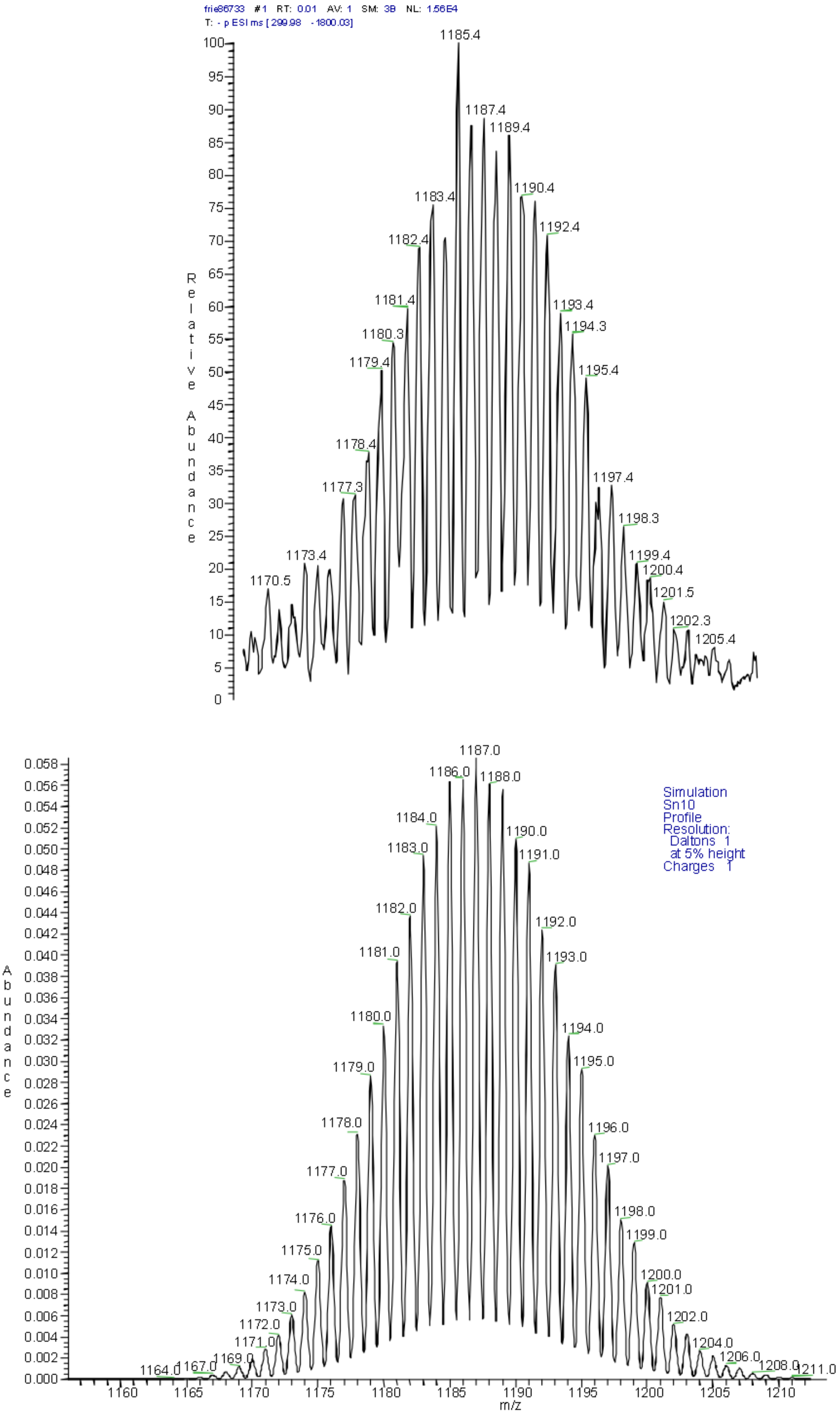

Figure 11 – Measured (top) and simulated (bottom) spectrum of Sn_{10}^{-} fragment

3 MASS SPECTROMETRY ANALYSIS

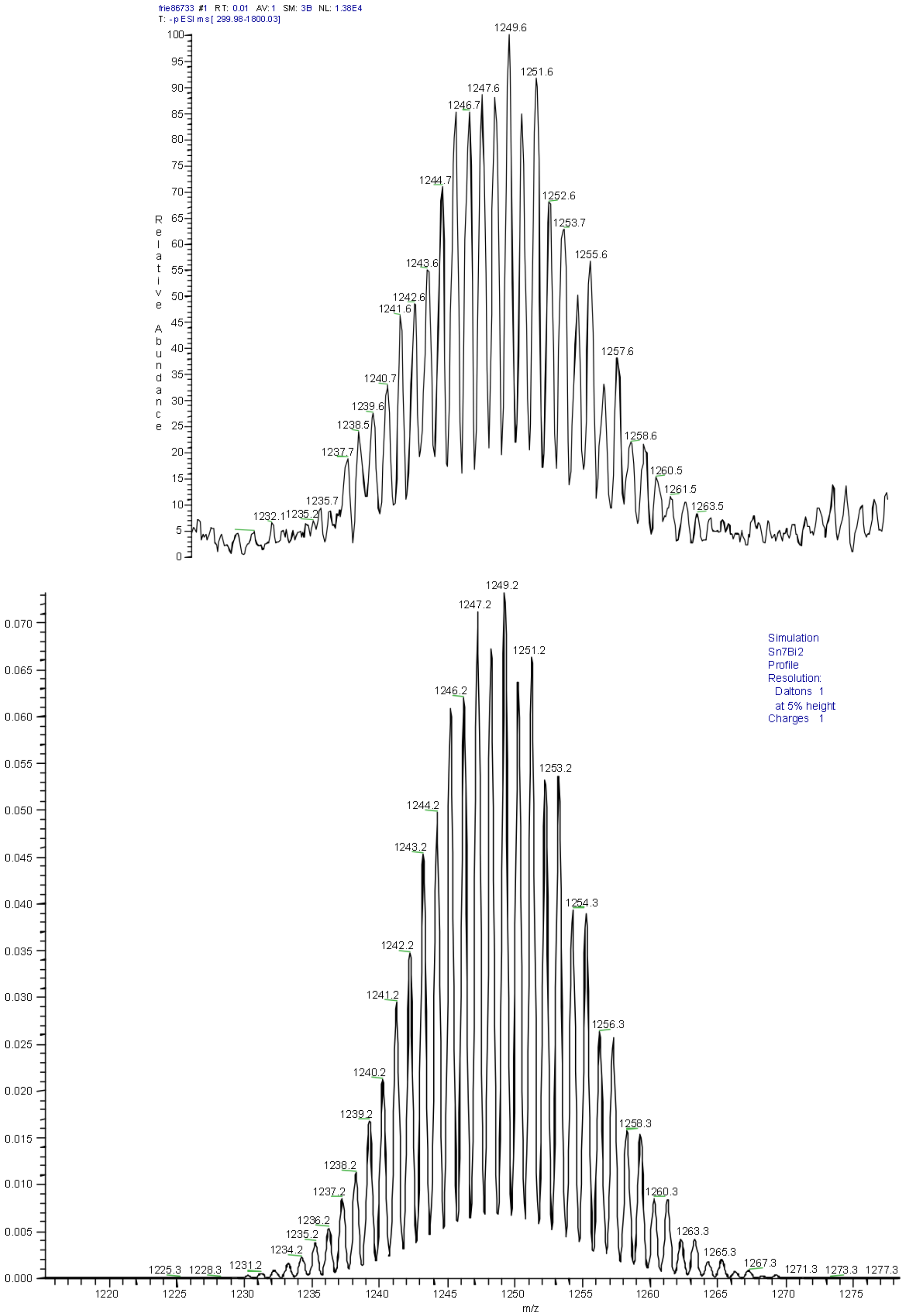

Figure 12 – Measured (top) and simulated (bottom) spectrum of $Sn_7Bi_2^-$ fragment

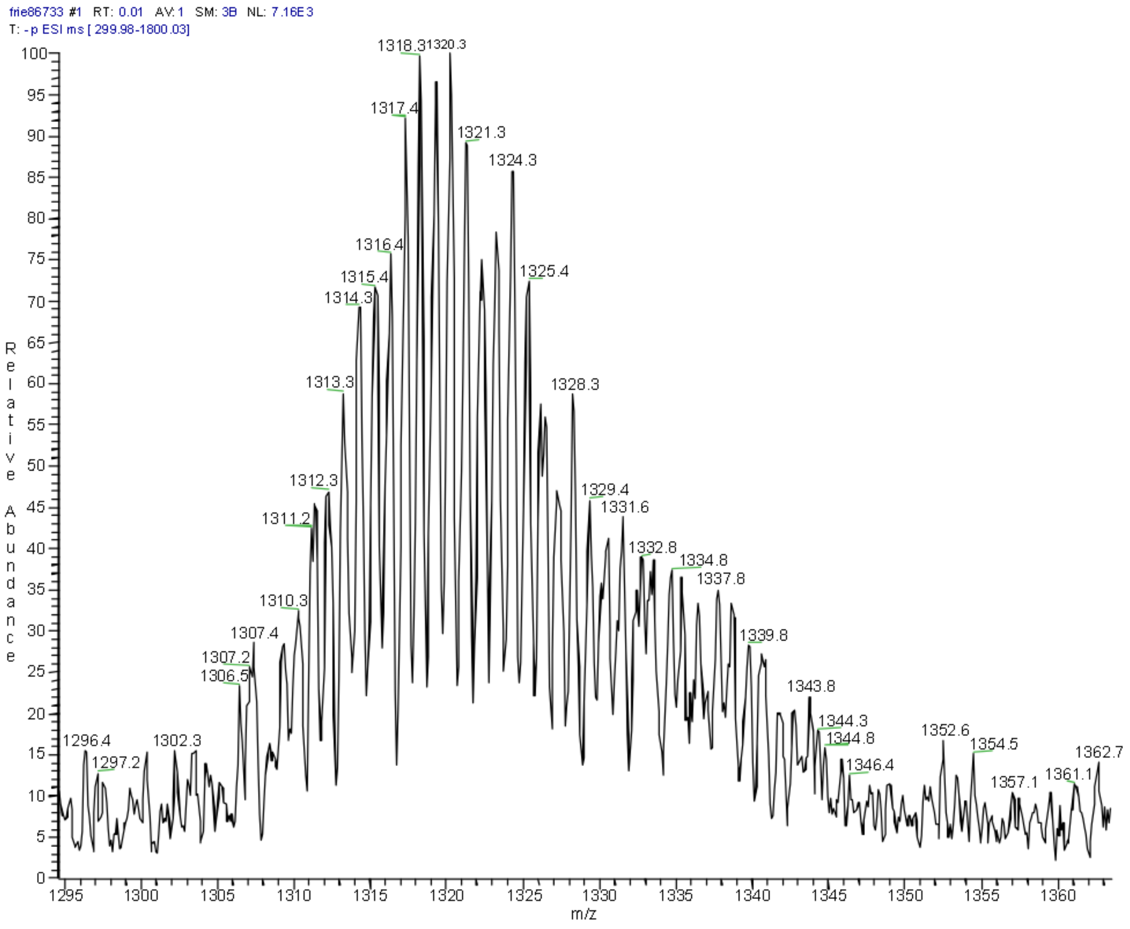

Figure 13 – Measured spectrum of $Sn_6Bi_3^-$ fragment (m/z = 1338.8), clearly overlayered by an unidentified signal, therefore, the simulated spectrum is not depicted

3.4 ESI mass spectrum of CsSnBi in presence of [18]crown-6

An overview of the ESI mass spectrum of CsSnBi that was measured with [18]crown-6 present in the solution, is depicted in Figure 14. Next to the usual single-charged species it was possible to detect double-charged species. Peaks of identified species (Table 4) are shown in Figures 15 - 22 together with the simulated isotopic patterns.

Table 4 – Identified fragments in ESI mass spectrum of CsSnBi in the presence of [18]crown-6

Species	**m/z**
Sn_{10}^{2-}	532.7
$Sn_2Bi_2^-$	655.8
$Sn_1Bi_3^-$	746.9
Sn_9^-	1068.3
Sn_8Bi^-	1158.4
Sn_{10}^-	1187.3
$Sn_7Bi_2^-$	1249.5
$Sn_6Bi_3^-$	1338.7

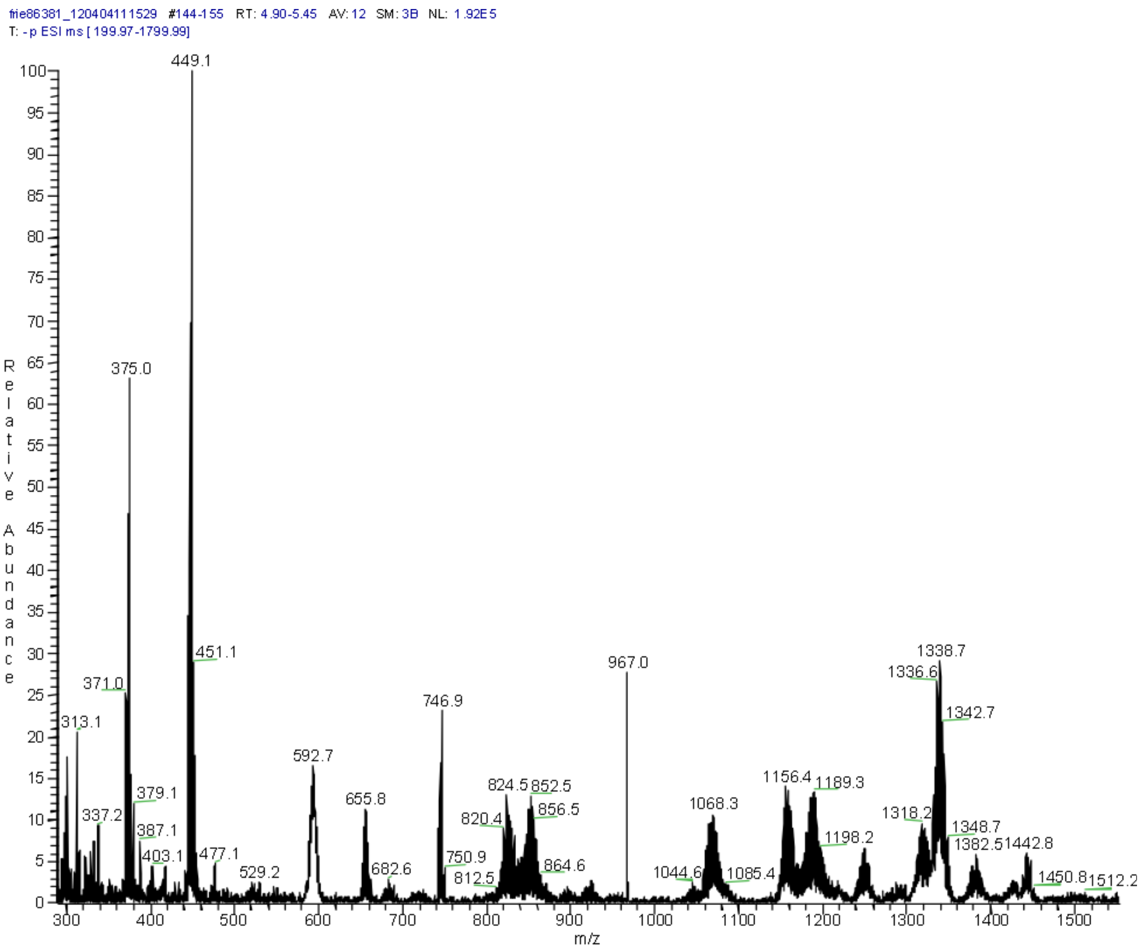

Figure 14 – ESI mass spectrum of a solution of CsSnBi in a mixture of ethylenediamine/dimethylformamide in the presence of [18]crown-6

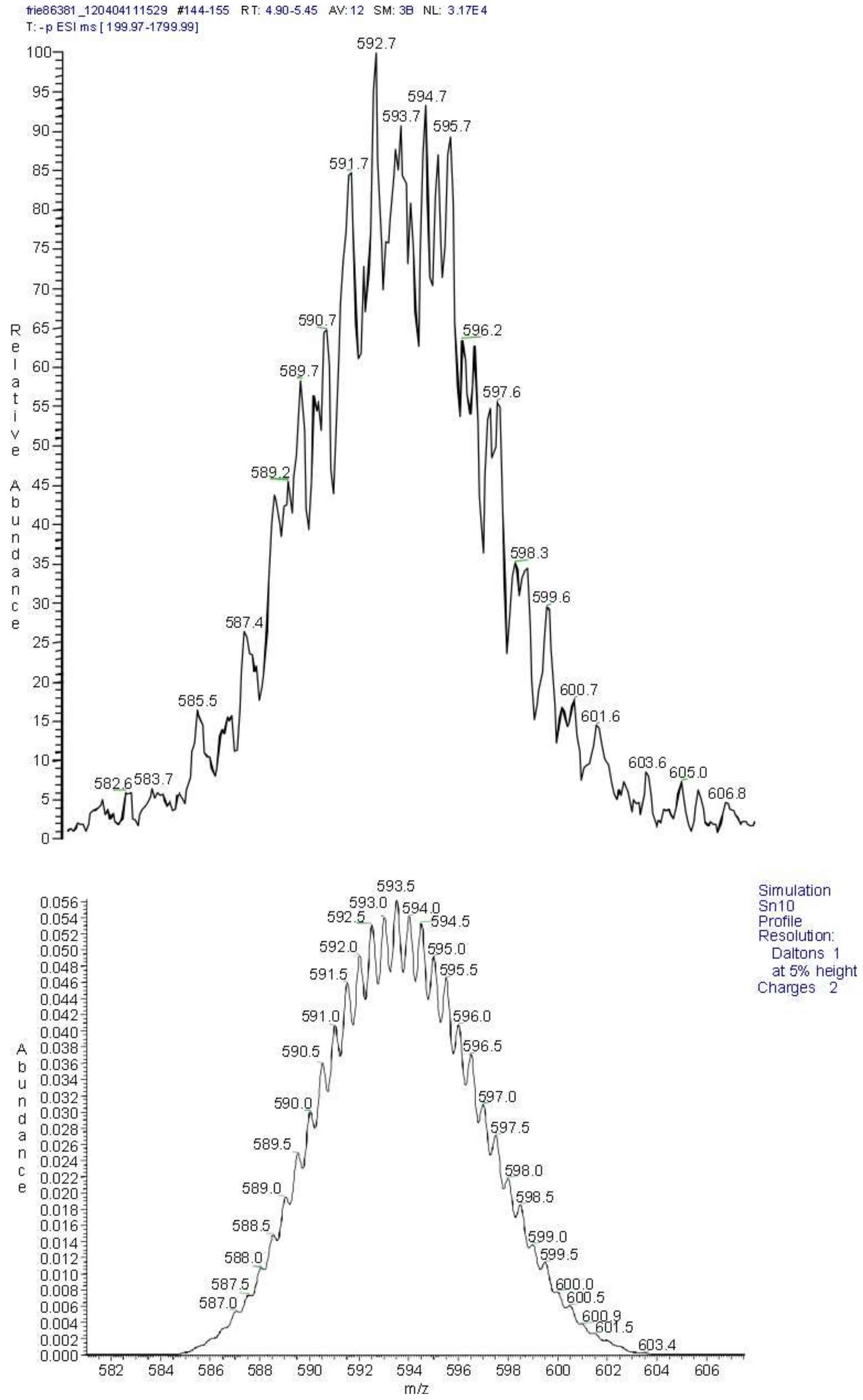

Figure 15 – Measured (top) and simulated (bottom) spectrum of Sn_{10}^{2-} fragment

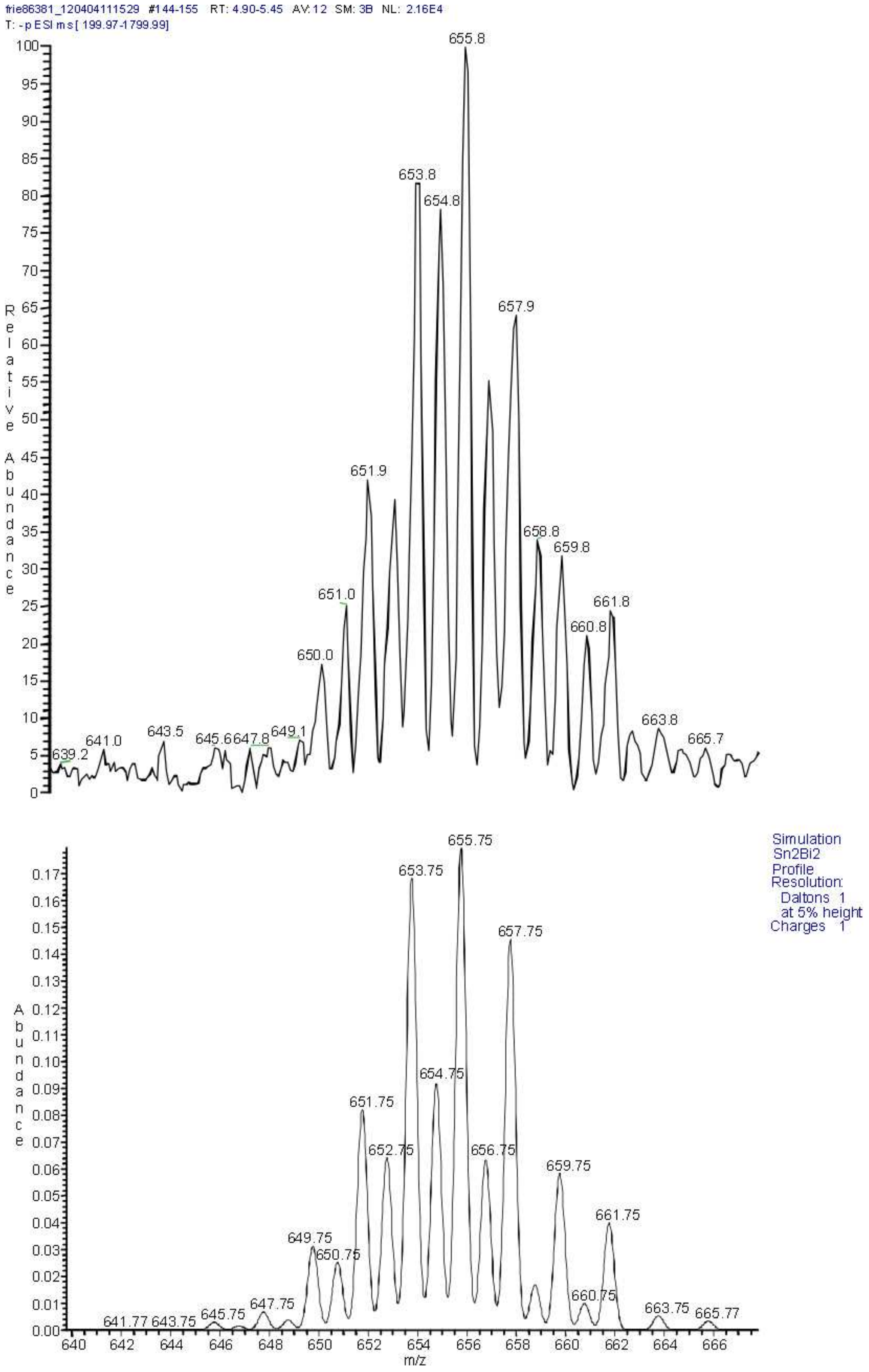

Figure 16 – Measured (top) and simulated (bottom) spectrum of $Sn_2Bi_2^-$ fragment

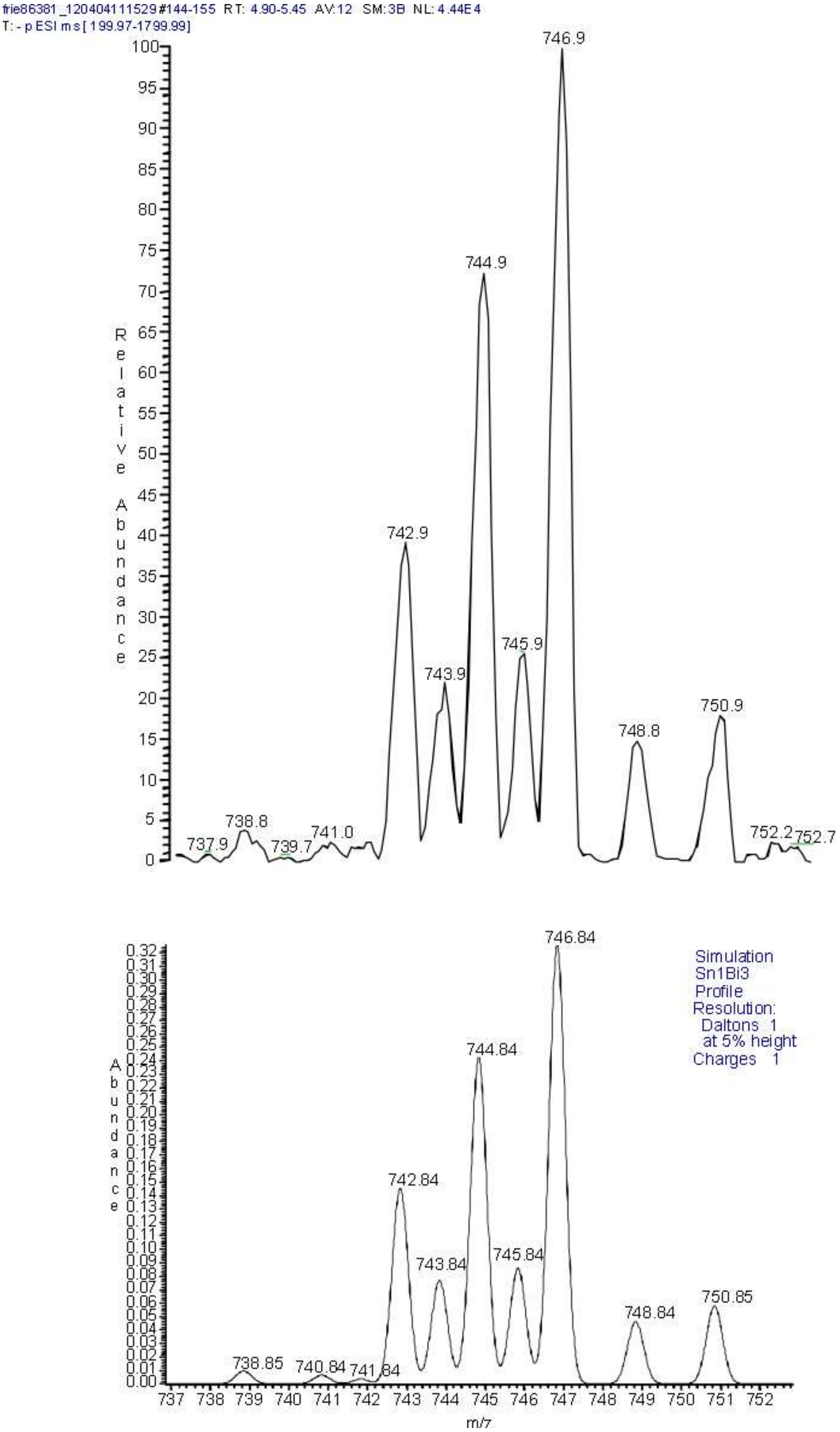

Figure 17 – Measured (top) and simulated (bottom) spectrum of $Sn_1Bi_3^-$ fragment

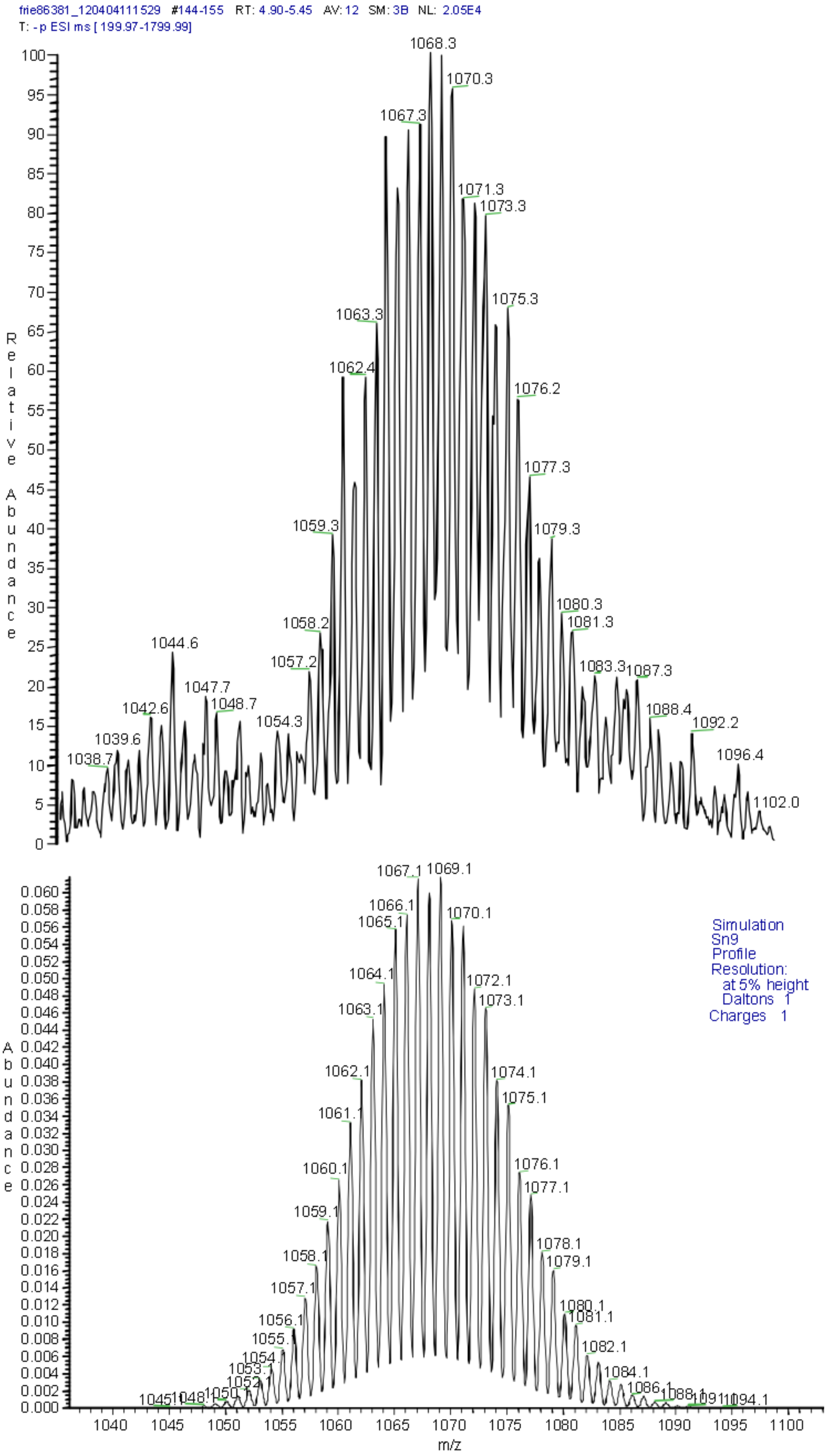

Figure 18 – Measured (top) and simulated (bottom) spectrum of Sn_9^- fragment

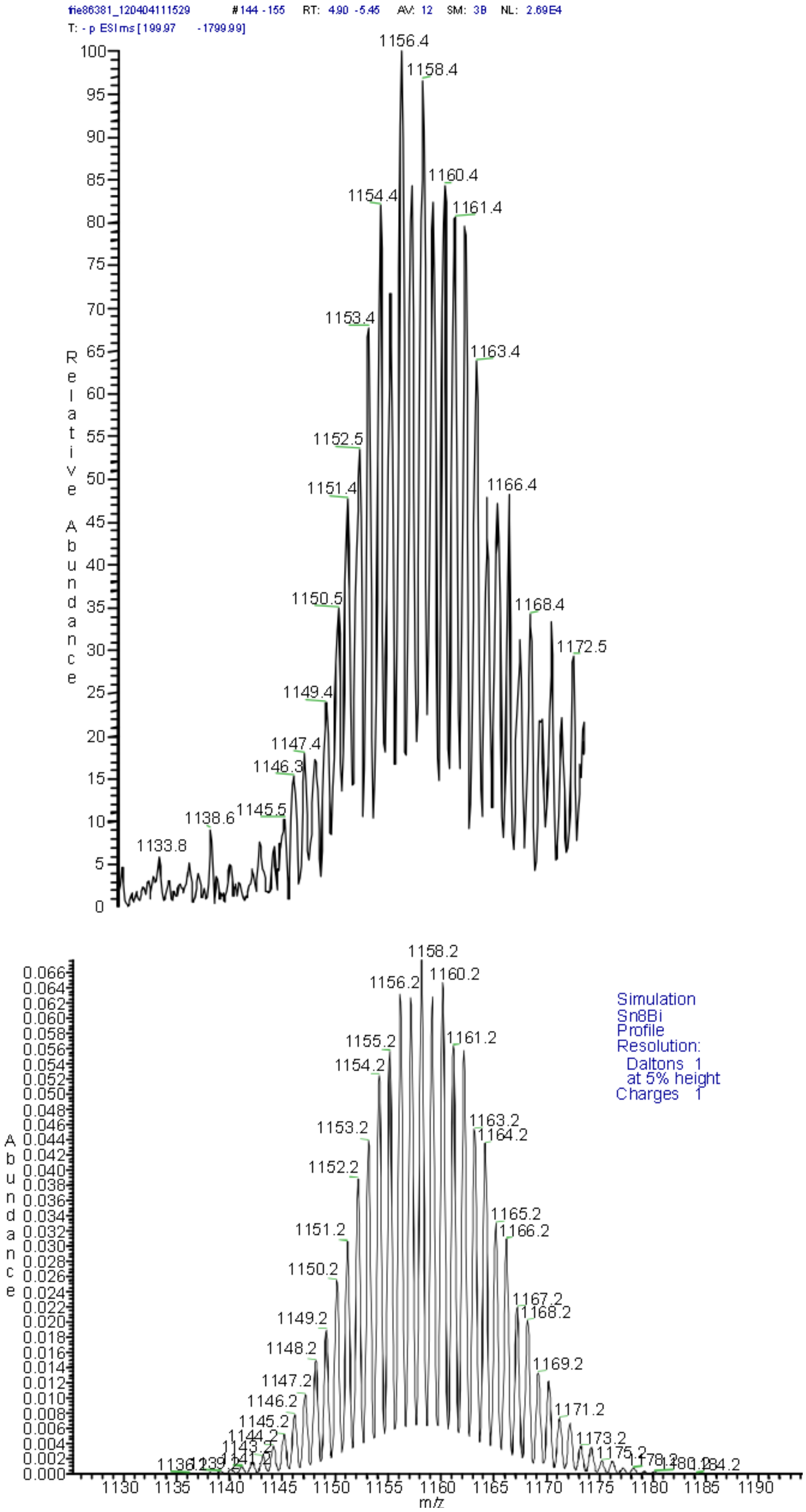

Figure 19 – Measured (top) and simulated (bottom) spectrum of Sn_8Bi^- fragment

3 MASS SPECTROMETRY ANALYSIS

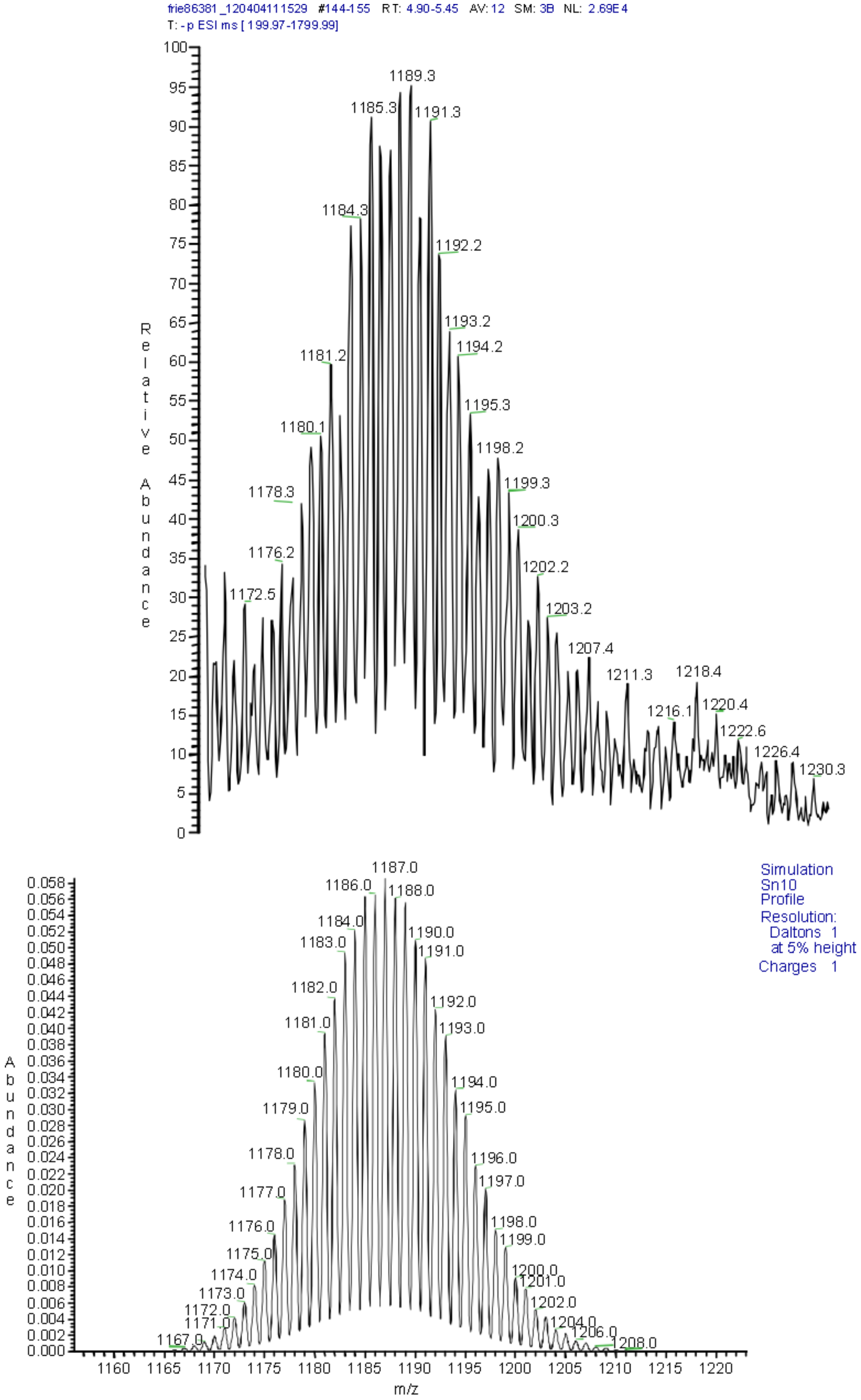

Figure 20 – Measured (top) and simulated (bottom) spectrum of Sn_{10}^- fragment

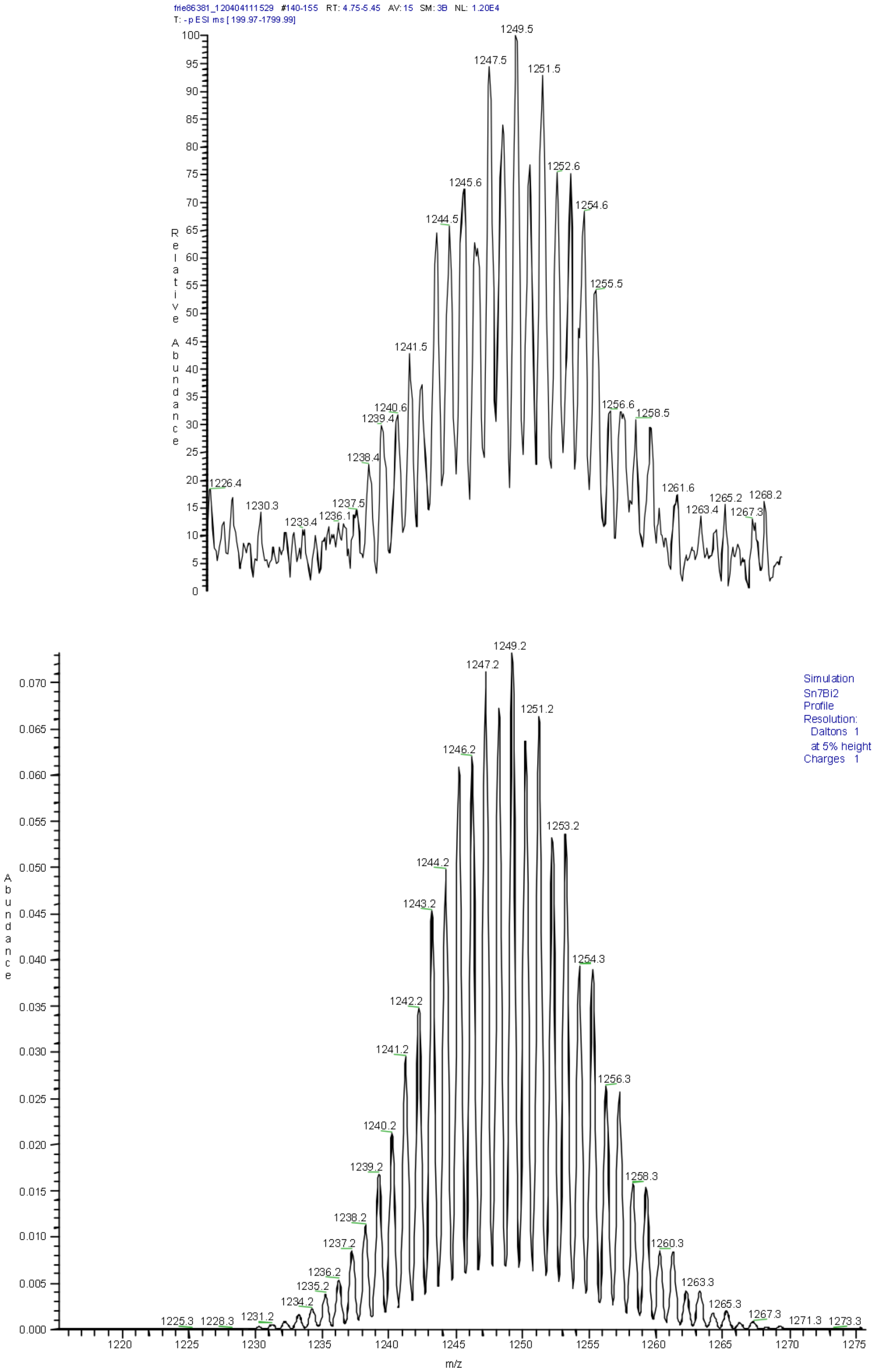

Figure 21 – Measured (top) and simulated (bottom) spectrum of $Sn_7Bi_2^-$ fragment

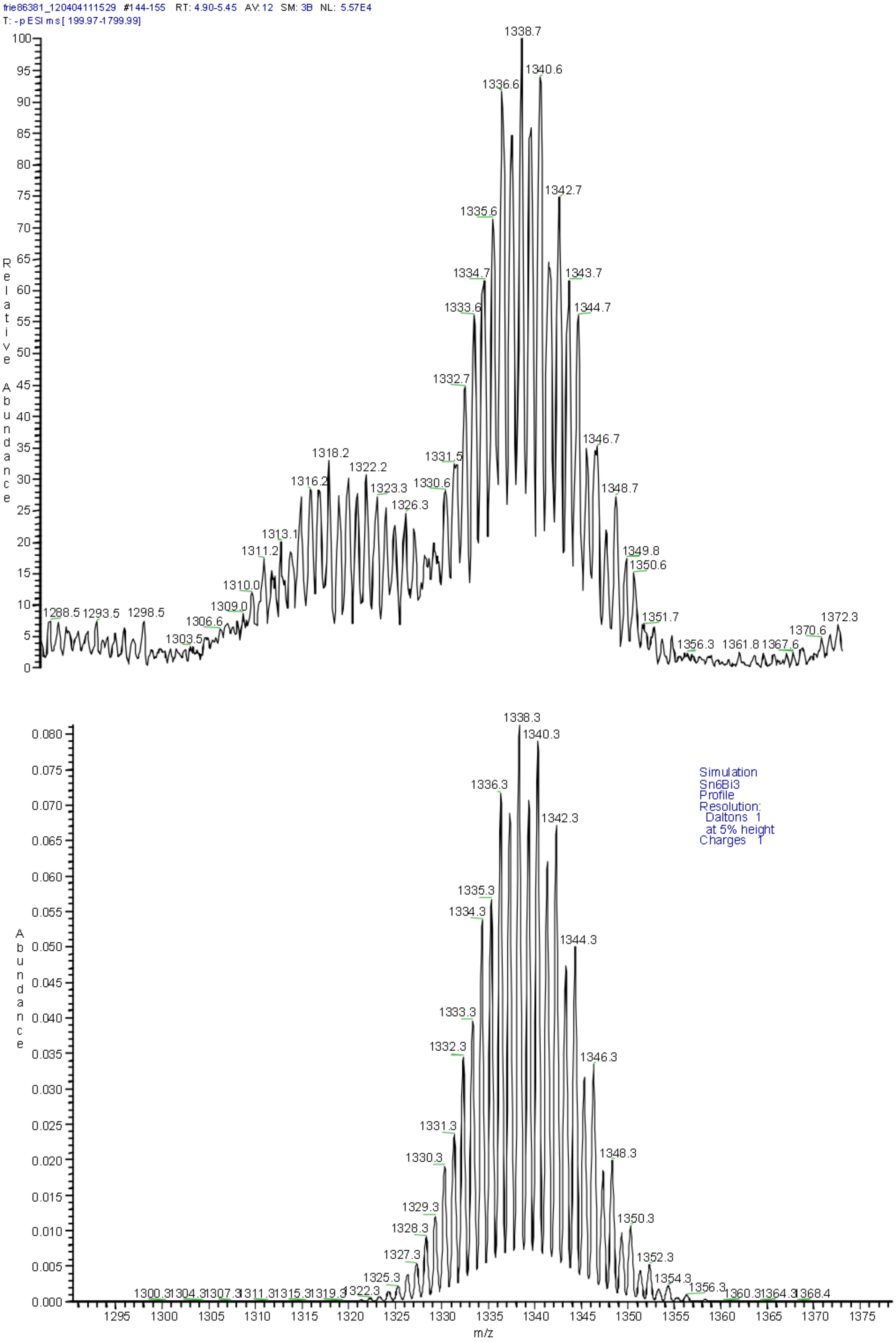

Figure 22 – Measured (top) and simulated (bottom) spectrum of $Sn_6Bi_3^-$ fragment

3.5 Mass spectrometry summary

In the mass spectrum of KSnBi and CsSnBi in ethylenediamine/ dimethylformamide solution neither the four atomic $[Sn_2Bi_2]^-$ nor the eightatom species $[Sn_4Bi_4]^-$ could be detected. Due to the bad resolution of the TSQ 7000 spectrometer it remains unclear whether the signal of $[Sn_3Bi_4]^-$ (m/z = 1191.6), which might be a precursor to $[Sn_4Bi_4]^{4-}$, is overlayered by the peak of $[Sn_{10}]^-$ (m/z = 1187.3). Dominant clusters are different nine-atom cages, which seem to be the most stable species in solution.
The addition of [18]crown-6 to the solution of CsSnBi contributes to the stabilization of the solution and the formation of smaller species such as $[Sn_2Bi_2]^-$ or $[Sn_1Bi_3]^-$. Indeed the presence of the sequestering agent has more effect on the detectable species in solution than the exchange of the counterion.

4 ^{119}NMR-spectroscopy

NMR spectroscopy was done on a Bruker Avance 600 spectrometer equipped with a 5 mm broadband triple resonance Z-gradient probe. The temperatures for all measurements were controlled by a Bruker BVTE 3900 temperature unit. ^{119}Sn measurements were carried out with a standard Bruker pulse program using 55 k number of scans for solutions of KSnBi or 80 k number of scans for solutions of CsSnBi, 2 dummy scans, TD=8 k and a relaxation delay of 0.3 s. Data were processed with the software Bruker TOPSPIN 2.1 [2] using the processing parameters SI=16 k, WDW=EM and LB=50 Hz. The chemical shifts are reported in ppm and are externally referenced to $SnMe_4$. For the measurements the original reaction solutions (solid state material + [18]crown-6 in liquid ammonia) were used.

In the spectrum of KSnBi (Figure 23, top) the singlet at -1746 ppm with J(^{119}Sn-^{117}Sn) = 1532 Hz is assigned to $[Sn_2Bi_2]^{2-}$. The upfield shift compared to the value of -1575 ppm with J(^{119}Sn-^{117}Sn) = 1638 Hz found by Wilson et al. [3] or of -1650 ppm reported by Dehnen et al. [4] is due to the presence of [18]crown-6 in solution [5] and the use of liquid ammonia as solvent instead of ethylenediamine. For the same reasons the signal at -1267 ppm with J(^{119}Sn-^{117}Sn) = 263 Hz, which is assigned to Sn_9^{4-}, is shifted about 60 ppm upfield with respect to the value found by Wilson et al. (-1210 ppm, J(^{119}Sn-^{117}Sn) = 263 Hz) [3]. The signal at -1244 ppm with J(^{119}Sn-^{117}Sn) = 615 Hz shows the best accordance with the simulated pattern of $[Sn_6Bi_3]^{-}$. The weak signal at -1192 ppm is supposed to

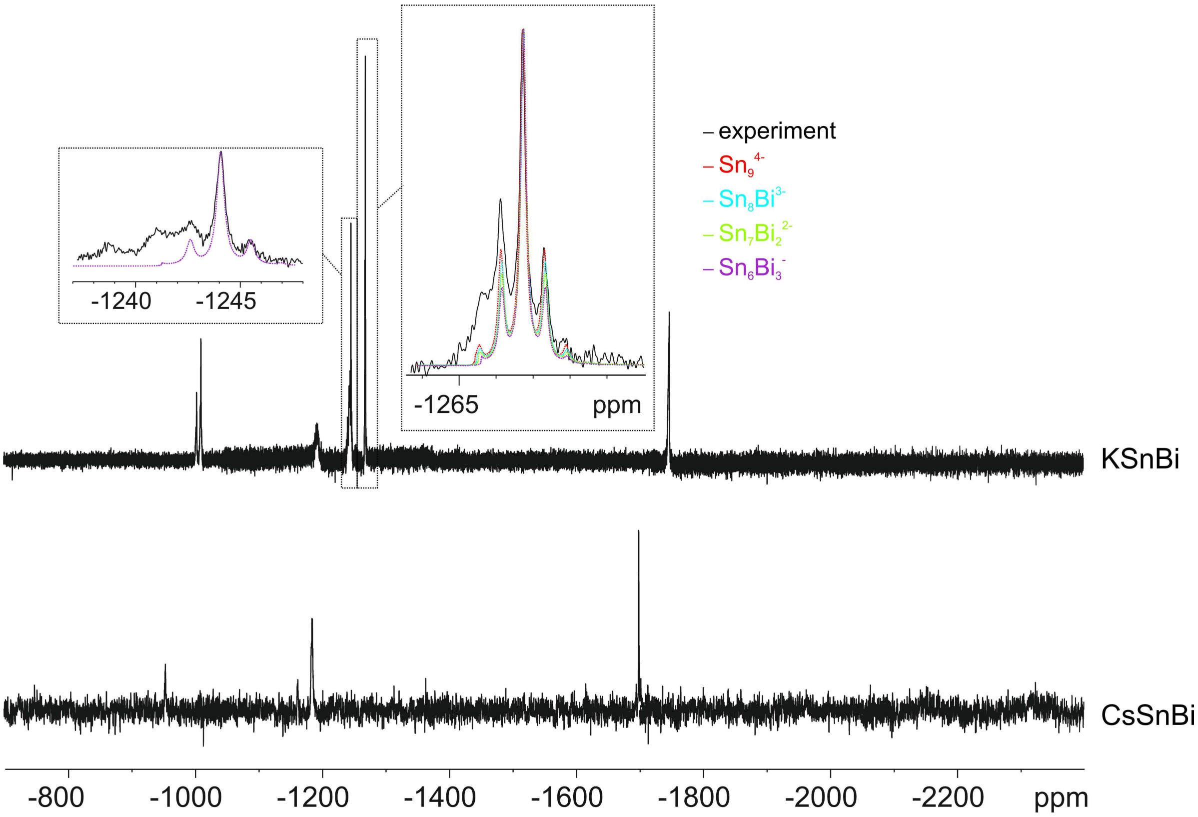

Figure 23 – Experimental (black) and simulated (coloured) ^{119}Sn NMR spectrum of KSnBi in liquid ammonia (top), experimenatal ^{119}Sn NMR spectrum of CsSnBi (bottom)

be another substituted Sn_9^{4-} species, but this cannot be proven. According to their chemical shifts, the singlets at −1011 ppm and −1004 ppm should belong to species with a lower formal negative charge per tin atom and might therefore belong to Sn_{10}^{2-}, which can be detected by ESI-MS in solution. But this is speculative due to the lack of further indicators.

For CsSnBi (Figure 23, bottom) four signals at −954 ppm, −1162 ppm, −1185 ppm and 1699 ppm ($J(^{119}Sn\text{-}^{117}Sn) = 1525$ Hz) can be detected. Due to the influence of the cation these signals are shifted to lower field in contrast to the KSnBi sample. Table 5 gives an overview over the signals detected in both samples and the assigned species.

Table 5 – ^{119}Sn-NMR signals common in KSnBi and CsSnBi solutions

Species	**δ(KSnBi) / ppm**	**δ(CsSnBi) / ppm**
$[Sn_2Bi_2]^{2-}$	−1746	−1699
Sn_9^{4-}	−1267	−1185
$[Sn_6Bi_3]^{-}$	−1244	−1162
unidentified	−1011	−954

5 Details of X-ray diffraction

Crystal preparation was done in perfluorinated ether oil (Galden® HT 230, Fa. Ausimont, USA), which was cooled in a stream of cold nitrogen. An appropriate crystal was mounted on a nylon loop of a Crystal Cap (CrystalCap Copper™ 14 mm with CryoLoop™ 20 μ 0.3-0.4 mm, Hampton Research, USA).

Both structures were solved using direct methods and refined with full matrix least squares against F^2 using SHELXS-97 and SHELXL-97 [6] within Olex^2 [7].

5.1 Compound 1

Single crystal X-ray diffraction for **1** was carried out on a Stoe IPDS I diffractometer at 123 K with Mo-K$_\alpha$-radiation ($\bar{\lambda}$ = 0.71073 Å).

The space group found for **1** by `XPREP` [8] and `Platon` [9] was *Pnma*. However, the solution in this space group resulted in disorder in one of the crown ether molecules and 20 or 95 systematic absent violations greater 3σ(I) occured for the glide planes *a* or *n*, indicating the wrong choice of the space group. Lowering the symmetry to space group $Pna2_1$, did not improve the model. A further reduction of symmetry to space group $P2_12_12_1$ and refinement as racemic twin resulted in a non-disordered model and much better quality factors (Table 6). Strong correlations between the carbon atoms of the crown ether molecules did not appear for this space group.
All hydrogen atoms were calculated geometrically and refined according to a riding model.

Table 6 – Quality factors of **1** for solutions in space groups *Pnma*, $Pna2_1$ and $P2_12_12_1$

	Pnma	$Pna2_1$	$P2_12_12_1$
*R*1 (all data)	0.0767	0.0817	0.0445
*wR*2 (all data)	0.1805	0.2048	0.0887
S	1.291	0.951	0.958
Flack	- - -	0.48(2)	0.503(7)
Data/parameter	3897/214	7451/195	7458/432

Table 7 – Crystallographic data for **1**

Compound	$[K([18]crown\text{-}6)]_2Sn_2Bi_2\cdot 2NH_3$
Empirical formula	C24 H54 Bi2 K2 N2 O12 Sn2
Formula weight / g·mol^{-1}	1296.23
Crystal size / mm	0.6 × 0.5 × 0.4
Crystal shape	plate
Crystal colour	reddish brown
Crystal system	orthorhombic
Space group	$P2_12_12_1$ (No. 19)
a / Å	10.4079(7)
b / Å	14.4988(10)
c / Å	27.679(2)
α	90°
β	90°
γ	90°
Volume / Å^3	4176.8(5)
Z	4
Calculated density / g·cm^{-3}	2.061
Absorption coefficient / mm^{-1}	9.831
Absorption correction	numerical
Max. / Min. transmission	0.3366 / 0.1635
θ-range for data collection	2.03°- 25.51°
Reflections collected / unique	52350 / 7458
Completeness to $\theta = 25.51$	95.2%
Data / restraints / parameters	7458 / 0 / 432
Goodness-of-fit on F^2	0.944
Final R indices [$I>2\sigma(I)$]	$R1 = 0.0352$, $wR2 = 0.0854$
R indices (all data)	$R1 = 0.0445$, $wR2 = 0.0887$
R_{int}	0.0958
Flack parameter	0.503(7)
Largest diff. peak and hole / $e\cdot$Å^{-3}	2.142 / -1.595

5 DETAILS OF X-RAY DIFFRACTION

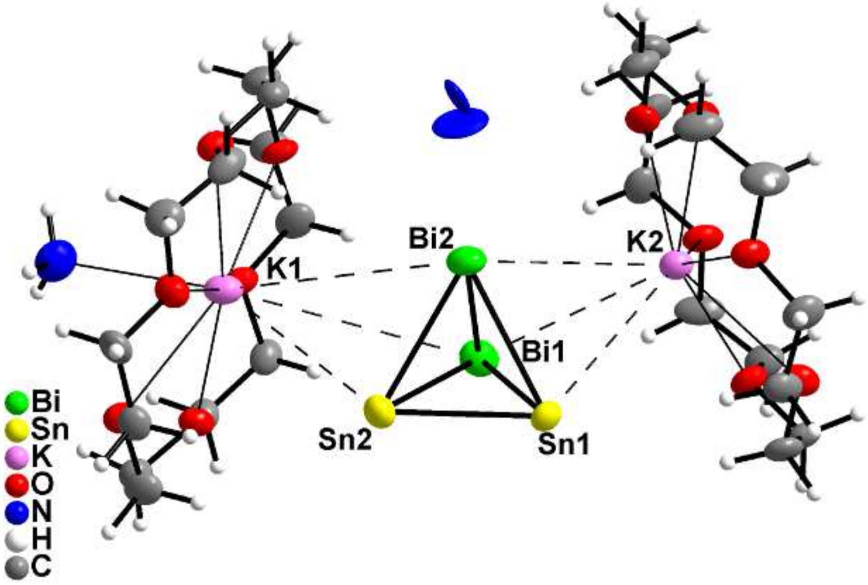

Figure 24 – Asymmetric unit of **1**. Anisotropic displacement ellipsoids at 50 % probability level.

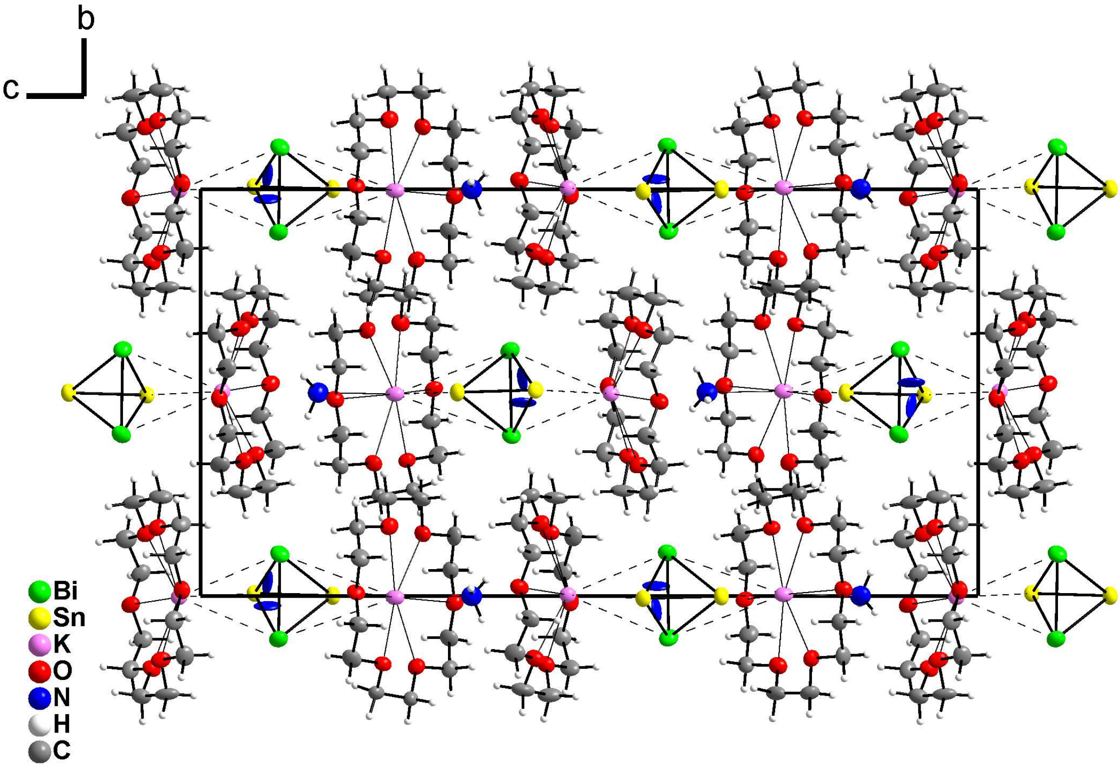

Figure 25 – Projection of **1** in crystallographical *a*-direction. Anisotropic displacement ellipsoids at 50 % probability level.

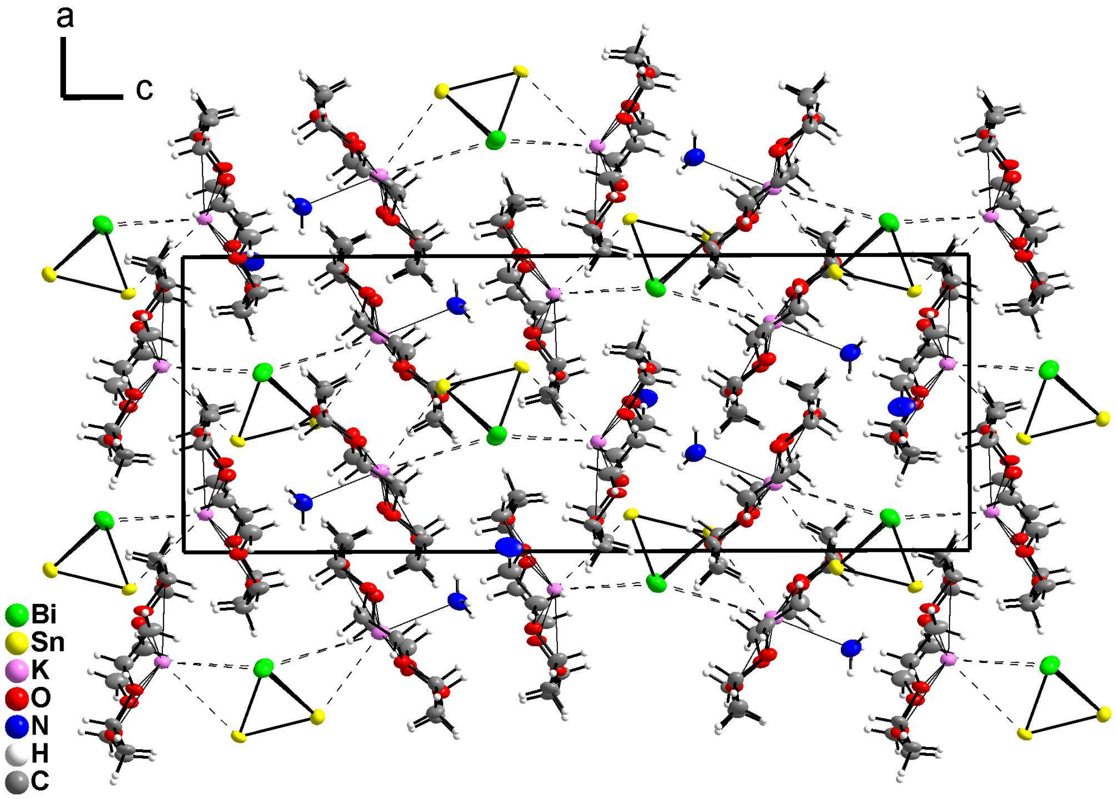

Figure 26 – Projection of **1** in crystallographical *b*-direction. Anisotropic displacement ellipsoids at 50 % probability level.

5.2 Compound 2

For **2** single crystal X-ray diffraction data were collected on a Gemini R Ultra (Oxford Diffraction Systems) at 123 K with Mo-K$_\alpha$-radiation ($\bar{\lambda}$ = 0.71073 Å).
The carbon atoms C7 and C8 were disordered and therefore treated with an EADP constraint.
Hydrogen atoms were calculated geometrically and refined according to a riding model.

Table 8 – Crystallographic data for **2**

Compound	$[Cs([18]crown\text{-}6)]_4Sn_4Bi_4 \cdot 12NH_3$
Empirical formula	C48 H132 Bi4 Cs4 N12 O24 Sn4
Formula weight / g·mol^{-1}	3103.98
Crystal size / mm	0.3 × 0.2 × 0.15
Crystal shape	block-shaped
Crystal colour	black
Crystal system	triclinic
Space group	$P\bar{1}$ (No. 2)
a / Å	15.5211(2)
b / Å	16.7664(2)
c / Å	21.7756(2)
α	72.442(1)°
β	87.793(1)°
γ	62.570(1)°
Volume / Å^3	4761.41(10)
Z	2
Calculated density / g·cm^{-3}	2.165
Absorption coefficient / mm^{-1}	9.964
Absorption correction	analytical
Max. / Min. transmission	0.354 / 0.149
θ-range for data collection	2.70°- 29.53°
Reflections collected / unique	691240 / 25670
Completeness to θ = 29.53	96.4%
Data / restraints / parameters	25670 / 0 / 932
Goodness-of-fit on F^2	1.047
Final R indices [I>2$\sigma(I)$]	$R1$ = 0.0406, $wR2$ = 0.0860
R indices (all data)	$R1$ = 0.0612, $wR2$ = 0.0931
R_{int}	0.0783
Largest diff. peak and hole / e·Å^{-3}	2.559 / −2.312

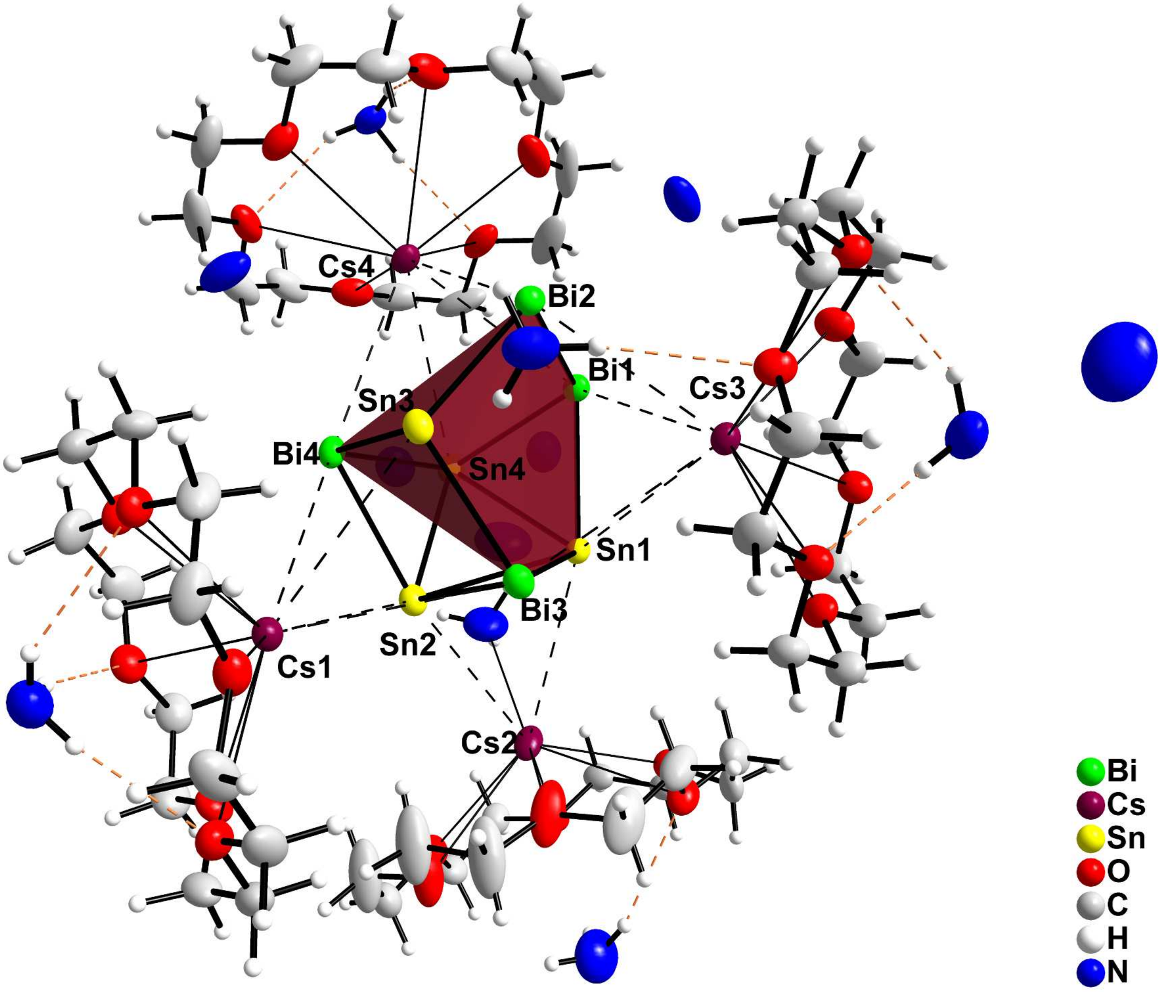

Figure 27 – Asymmetric unit of **2**. Anisotropic displacement ellipsoids at 50 % probability level.

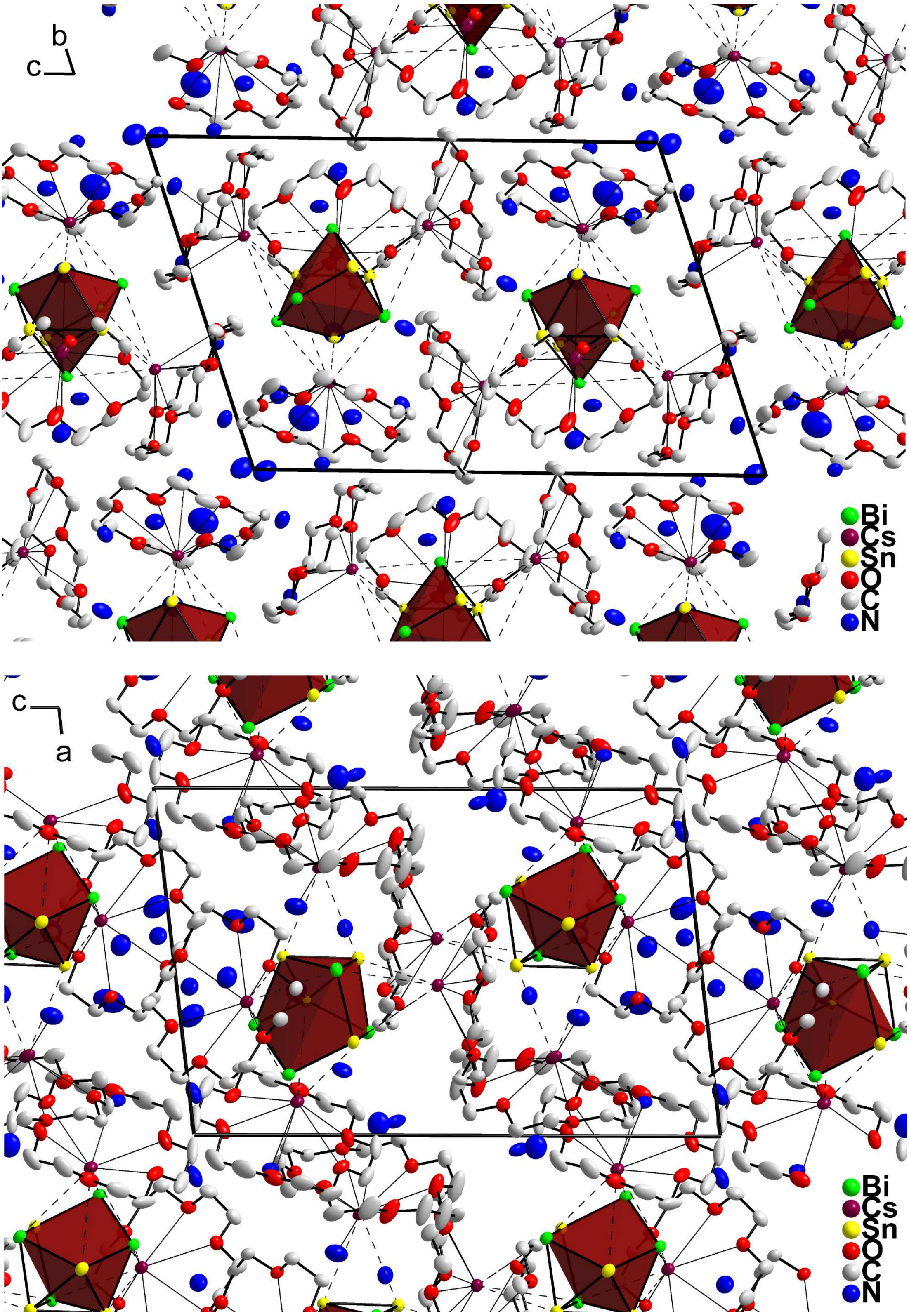

Figure 28 – Projection of **2** in crystallographical *a*-direction (top) and *b*-direction (bottom), hydrogen atoms not depicted. Anisotropic displacement ellipsoids at 50 % probability level.

6 Theoretical Studies

Ab-initio calculations were done on Hartree Fock level using the program system TURBOMOLE [10]. Basis sets for tin and bismuth atoms were of def2-TZVP quality (TZVP = Triple Zeta Valence plus Polarization). For the consideration of relativistic effects and to minimize the computational effort effective core potentials (Sn: ecp-28, Bi: ecp-60) were used. The high negative charge of the $Sn_4Bi_4^{4-}$ anion was compensated for by employment of the COSMO model. The chosen ε = 16.9 corresponds to that of ammonia. The optimization of the geometric structure (Table 9) was performed without symmetry restrictions (C1). Electron localization function calculations (ELF) were carried out with the program DGRID [11] (Figure 29). Additionally Figure 30 shows the valence orbitals obtained from the TURBOMOLE calculations. For the representation of the orbitals the program gOpenMol [12, 13] was used.

Table 9 – Optimized and experimental atomic distances in $Sn_4Bi_4^{4-}$

atoms	**d_{opt} / Å**	**d_{exp} / Å**	**atoms**	**d_{opt} / Å**	**d_{exp} / Å**
Sn3 - Bi2	2.8642	2.8647	Sn1 - Bi1	2.9594	2.9705
Sn3 - Bi3	2.9833	2.9799	Sn1 - Sn4	3.1363	3.1360
Sn3 - Bi4	2.9786	2.9826	Sn2 - Bi4	2.9886	3.0171
Bi2 - Bi1	3.0313	3.0307	Sn2 - Bi3	3.0173	2.9884
Bi3 - Sn1	2.9497	2.9542	Sn2 - Sn4	3.0515	3.0925
Bi4 - Sn4	2.9536	2.9495	Sn2 - Sn1	3.0932	3.0510
Bi1 - Sn4	2.9595	2.9717			

The experimental Sn-Sn bond lengths in compound **2** are distinctly longer than those found for compound **1**. ELF calculations show a three centre bond within the tin triangle, which can explain the observed elongation. The valence orbitals, especially HOMO-3 and HOMO-15 (Figure 30) indicate the presence of a three centre bond and thus support the result of the ELF calculation.

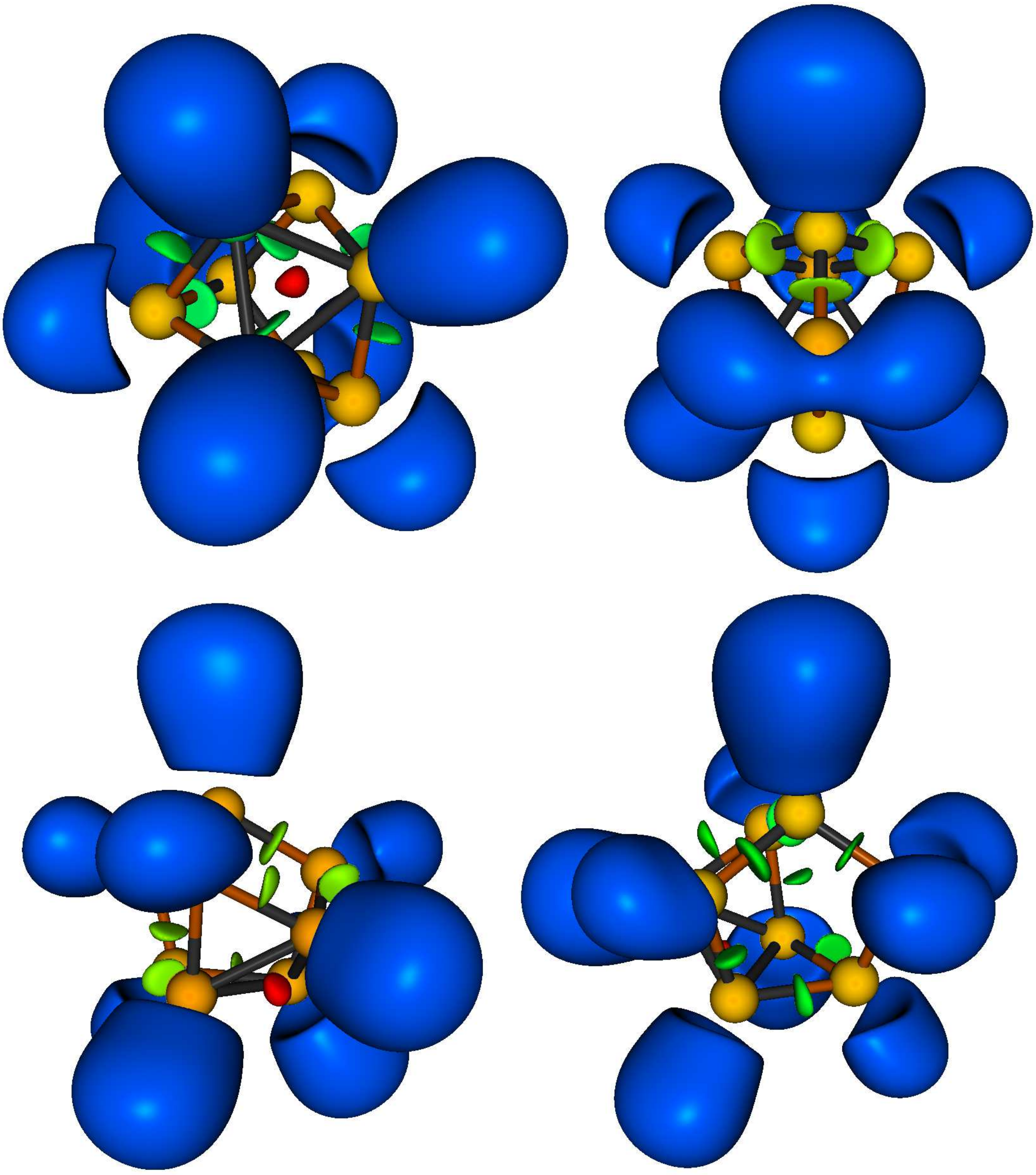

Figure 29 – ELF of $Sn_4Bi_4^{4-}$; η = 0.66, monosynaptic core basins yellow, monosynaptic valence basins blue, disynaptic valence basins green and trisynaptic valence basins red.

HOMO
ε = - 3.966 eV

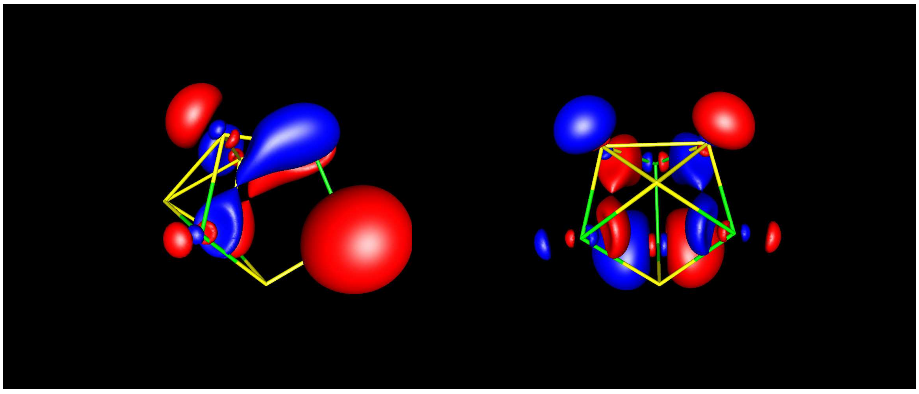

HOMO-1
ε = - 4.070 eV

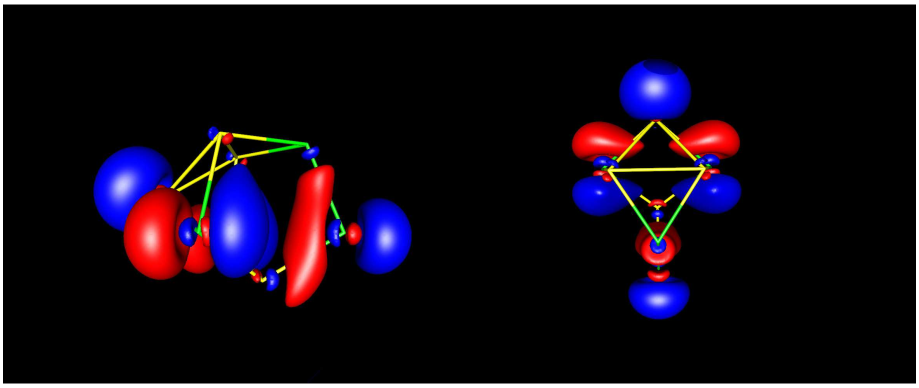

HOMO-2
ε = - 4.112 eV

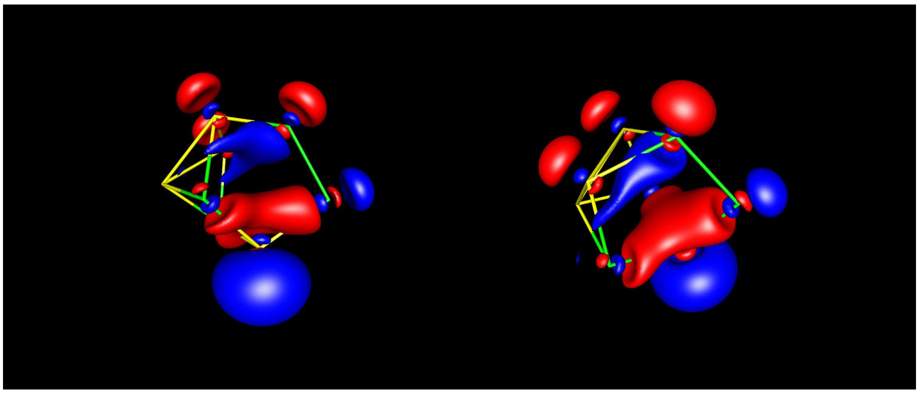

HOMO-3
ε = - 4.614 eV

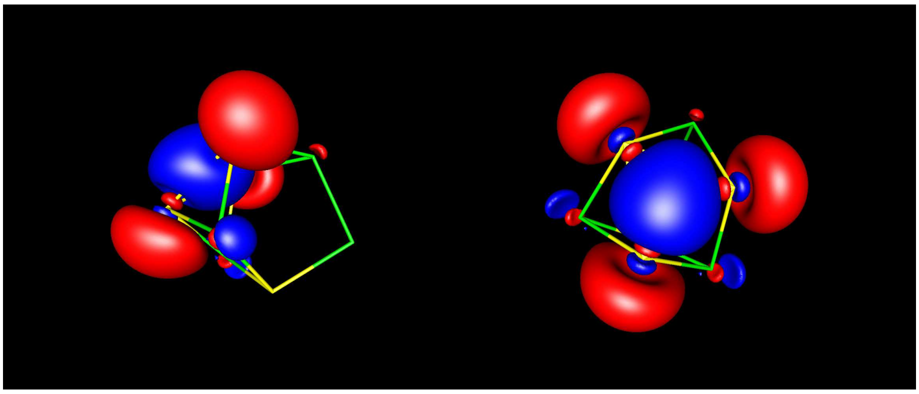

Electronic Supplementary Material (ESI) for Chemical Communications

HOMO-4
ε = - 4.662 eV

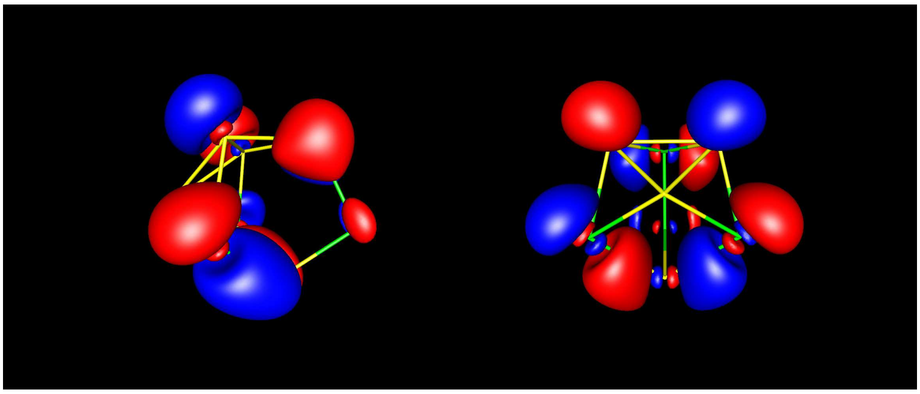

HOMO-5
ε = - 4.837 eV

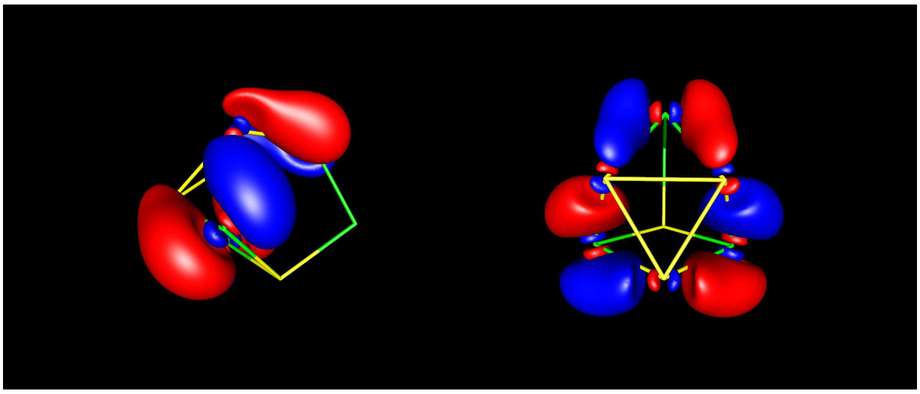

HOMO-6
ε = - 5.137 eV

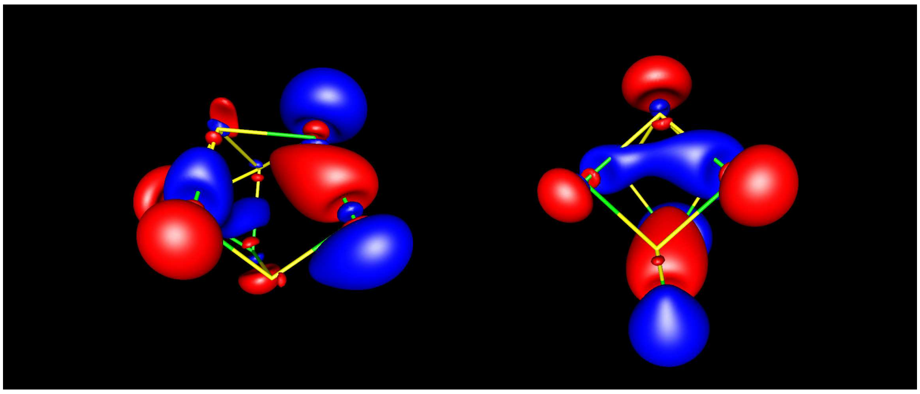

HOMO-7
ε = - 5.138 eV

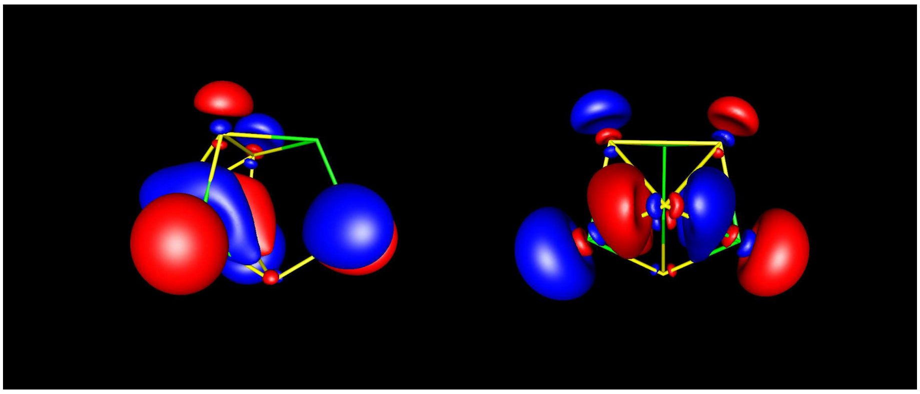

HOMO-8
ε = - 5.767 eV

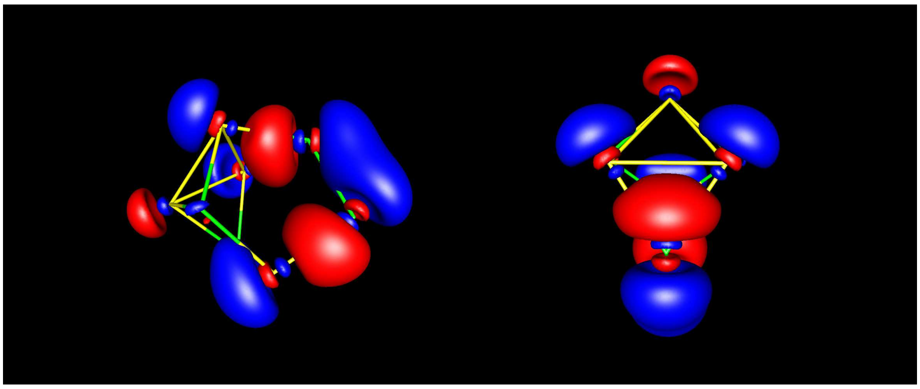

HOMO-9
ε = - 6.156 eV

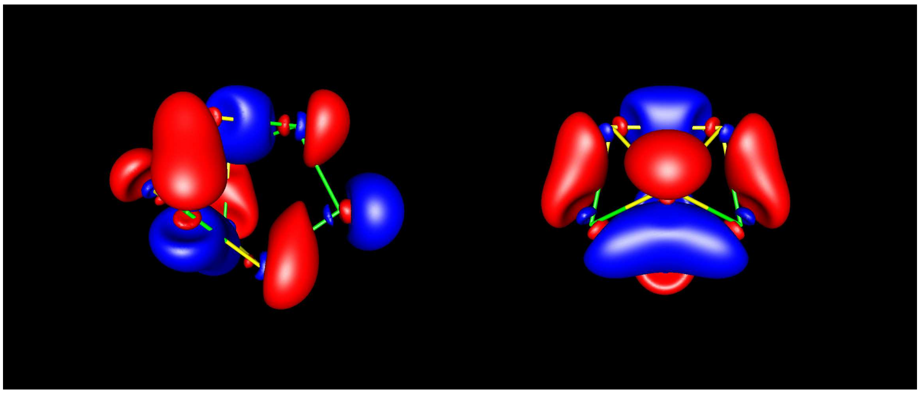

HOMO-10
ε = - 6.884 eV

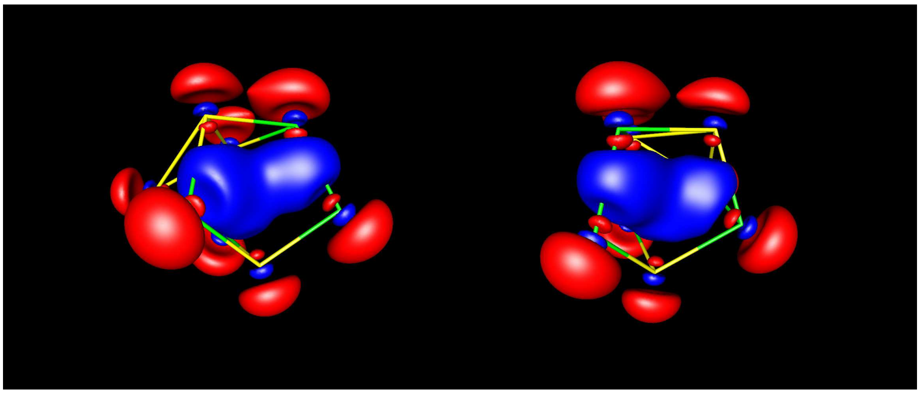

HOMO-11
ε = - 6.942 eV

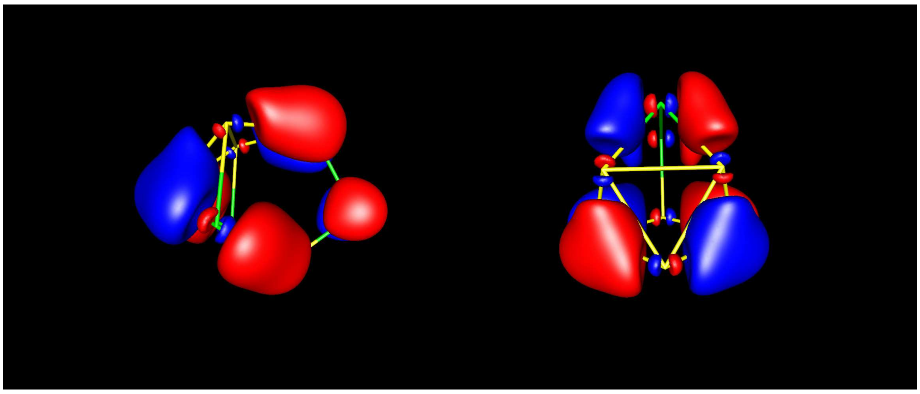

HOMO-12
ε = - 11.107 eV

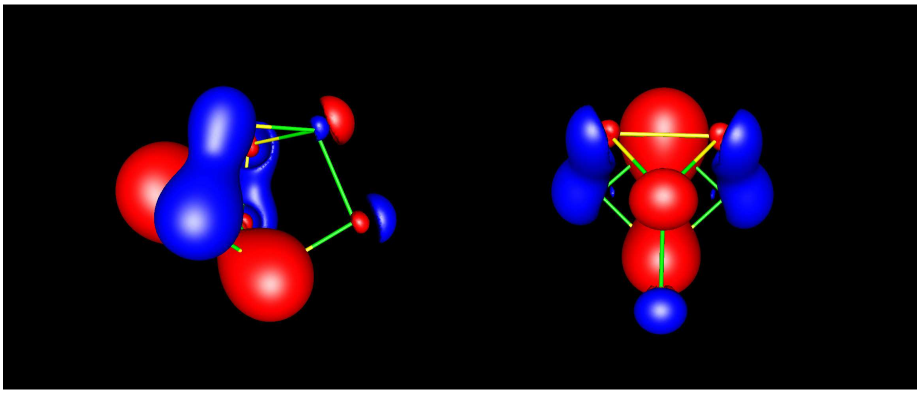

HOMO-13
ε = - 11.358 eV

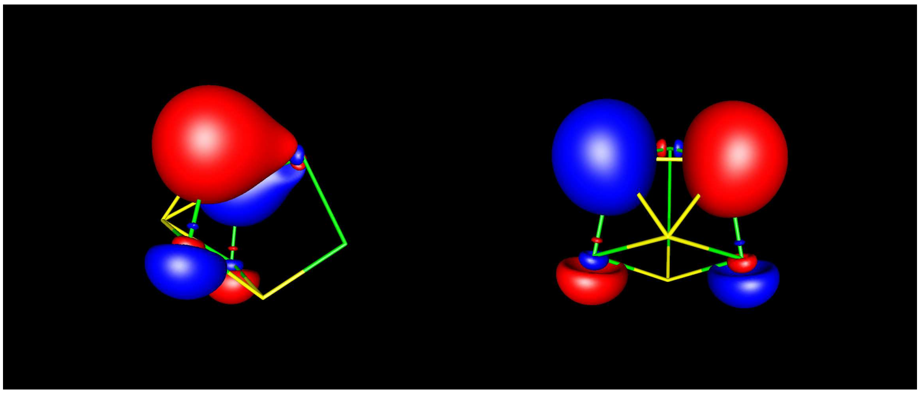

HOMO-14
ε = - 11.530 eV

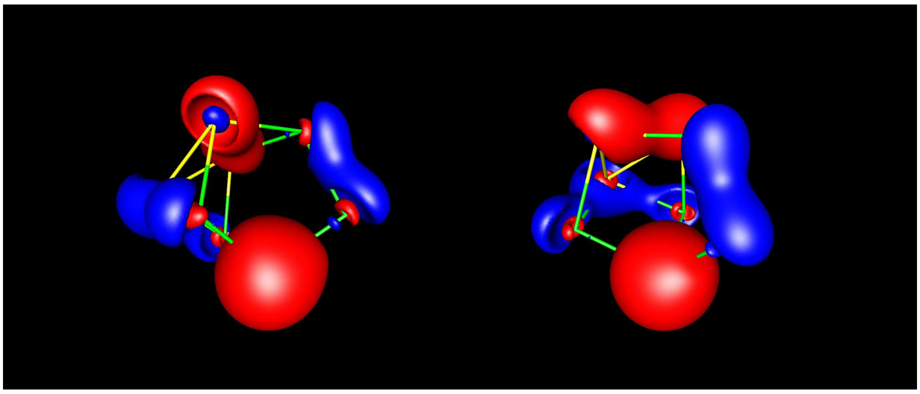

HOMO-15
ε = - 13.149 eV

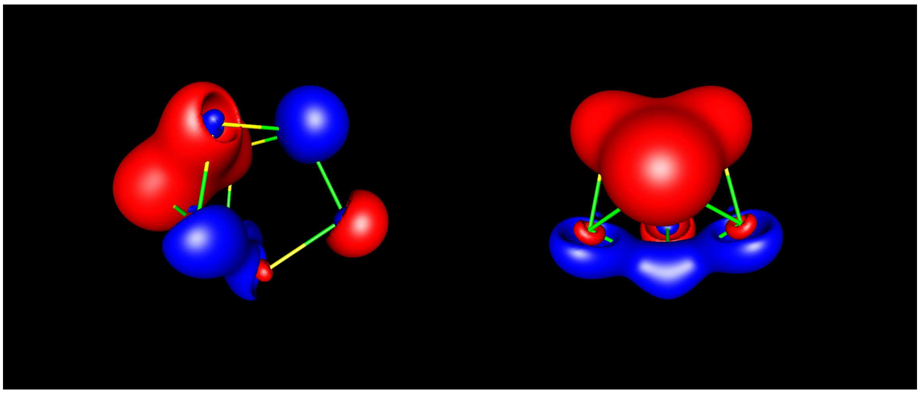

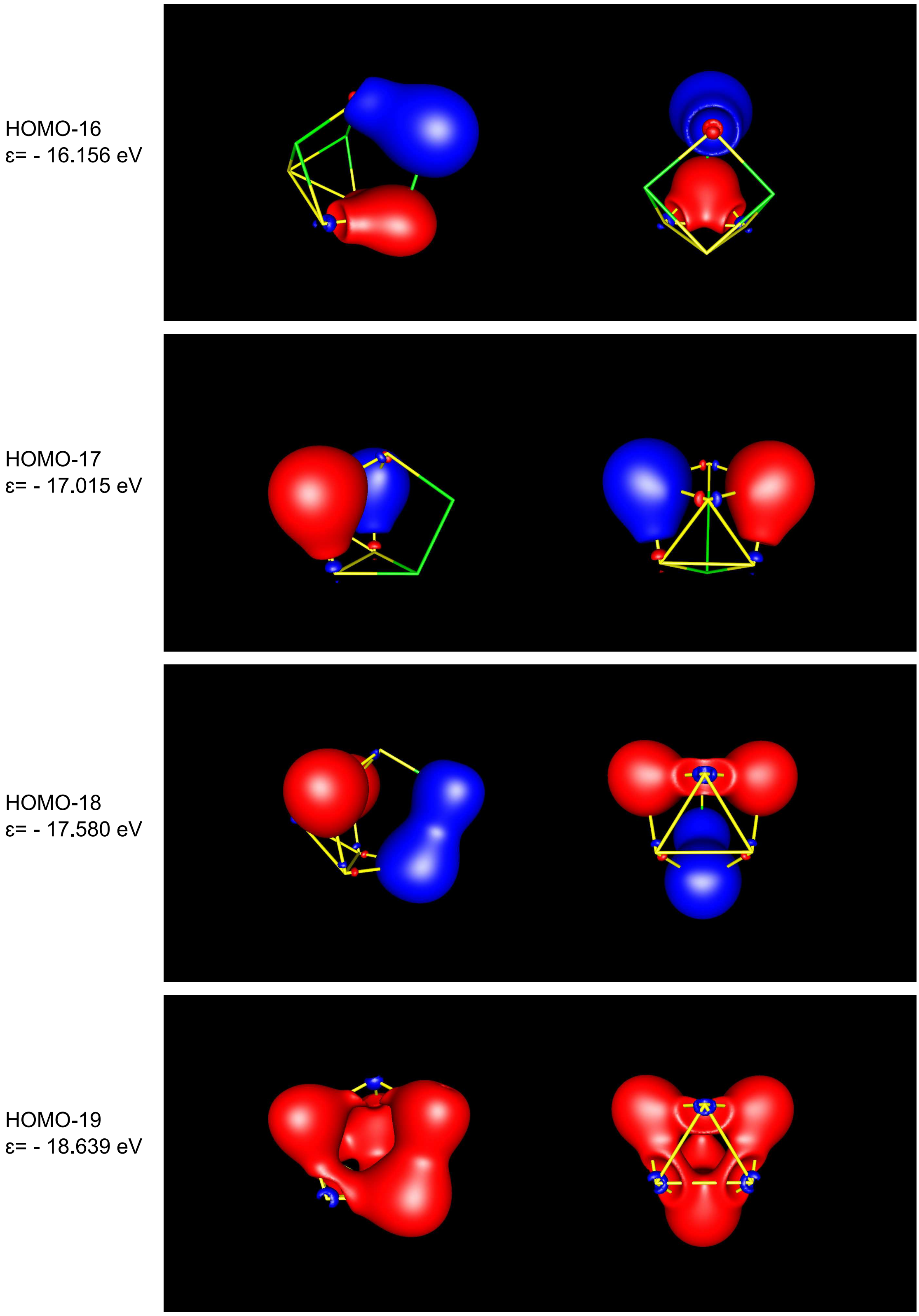

Figure 30 – Valence orbitals of $Sn_4Bi_4^{4-}$

References

[1] E. Zintl, A. Harder, *Phys. Chem.* **1932**, *16*, 206–212.

[2] Bruker,TOPSPIN,Version 2.1, **2010**.

[3] W. L. Wilson, R. W. Rudolph, L. L. Lohr, R. C. Taylor, P. Pyykkö, *Inorg.Chem.* **1986**, *25*, 1535–1541.

[4] F. Lips, S. Dehnen, *Angew. Chem.* **2009**, *121*, 6557–6560.

[5] F. S. Kocak, D. O. Downing, P. Y. Zavalij, Y.-F. Lam, A. N. Vedernikov, B. Eichhorn, *J. Am. Chem. Soc.* **2012**, *134*, 9733–9740.

[6] G. Sheldrick, SHELX97 - Programs for the solution and refinement of crystal structures, Universität Göttingen, **1997**.

[7] O. V. Dolomanov, L. J. Bourish, R. J. Gildea, J. A. K. Howard, H. Puschmann, *J. Appl. Cryst.* **2009**, *42*, 339–341.

[8] Bruker Analytical X-ray Systems, XPREP - Reciprocal space exploration, Version 2005/2 for Windows, **2005**.

[9] A. L. Spek, PLATON - A Multipurpose Crystallographic Tool, Utrecht University (NL), **2005**.

[10] TURBOMOLE V6.26 2010, a development of University of Karlsruhe and Forschungszentrum Karlsruhe GmbH, 1989-2007, TURBOMOLE GmbH, since 2007, **2010**.

[11] M. Kohout, DGrid, version 4.6, Radebeul, **2011**.

[12] L. Laaksonen, *J. Mol. Graph.* **1992**, *10*, 33–34.

[13] D. L. Bergman, L. Laaksonen, A. Laaksonen, *J. Mol. Graph. Model.* **1997**, *15*, 301–306.